MULTI-SCALE INDENTATION HARDNESS TESTING;

A CORRELATION AND MODEL

A Thesis

by

DAMON WADE BENNETT

Submitted to the Office of Graduate Studies of
Texas A&M University
in partial fulfillment of the requirements for the degree of

MASTER OF SCIENCE

August 2008

Major Subject: Mechanical Engineering

MULTI-SCALE INDENTATION HARDNESS TESTING;

A CORRELATION AND MODEL

A Thesis

by

DAMON WADE BENNETT

Submitted to the Office of Graduate Studies of
Texas A&M University
in partial fulfillment of the requirements for the degree of

MASTER OF SCIENCE

Approved by:

Chair of Committee,	Hong Liang
Committee Members,	Richard Griffin
	William D. McCain Jr.
Head of Department,	Dennis L. O'Neal

August 2008

Major Subject: Mechanical Engineering

ABSTRACT

Multi-scale Indentation Hardness Testing;

A Correlation and Model. (August 2008)

Damon Wade Bennett, B.S., Oklahoma State University

Chair of Advisory Committee: Dr. Hong Liang

This thesis presents the research results of a correlation and model based on nano and macroindentation hardness measurements. The materials used to develop and test the correlation include bulk tantalum and O1 tool steel. Following the literature review and a detailed description of the experimental techniques, the results of the nanoindentation hardness measurements are presented. After applying the methods and correlation recommended here, the results should give an accurate value of hardness in the Vickers scale for microstructural features that are too small to be precisely and exclusively measured using the traditional macroindentation hardness technique. The phenomena and influential factors in nanoindentation hardness testing are also discussed. These phenomena and theories are consistent with the microstructural behavior predicted in the Nix and Gao model for mechanism-based strain gradients. Implementing the correlation factors and/or correlation curve, accurate results can be found for metals over a broad hardness range. Initially, this research may impact the pipeline division of the petroleum industry by providing a correlation to the Vickers scale for nanoindentation

testing of microstructural features. This thesis may also provide a research methodology to develop hardness correlations for materials other than metals.

This thesis consists of eight chapters. Following an introduction in Chapter I, the research motivations and objectives are highlighted in Chapter II. Chapter III explains the multi-scale indentation techniques used in this thesis and Chapter IV presents the materials preparation techniques used. Then, the results are presented in Chapter V, followed by the factors affecting nanoindentation hardness in Chapter VI. Finally, Chapters VII and VIII reveal the indentation contact analysis, correlation, and conclusions of this research, respectively.

ACKNOWLEDGEMENTS

I would like to thank my committee chair, Dr. Liang, and committee members, Dr. Griffin and Dr. McCain for their guidance and support throughout this research. Thanks also goes to Dr. Fairchild, Dr. Kumar, Dr. Macia, Dr. Nissley and Dr. Cheng; members of the Offshore, Arctic, and Pipeline Division of the Upstream Research Company of ExxonMobil for their support throughout this research. Thanks also goes to the ExxonMobil Production Company, Operations Technical Reservoir, United States Production managers and supervisors for their support throughout graduate school.

I would like to thank my friends and colleagues in Dr. Liang's research group and the faculty and staff in the mechanical engineering department for making my time at Texas A&M University a great and memorable experience. More specifically, a special thanks to Aracely Rocha, Rodrigo Cooper, Ke Wang, and Gang Liang for assisting in the nanoindentation testing. Another special thanks goes to Dr. Julien Fontaine from Ecole Centrale de Lyon for support of nanoindentation testing. To all, although we may pursue different careers, I am convinced that our paths will cross again by virtue of our continued focus on advanced technologies.

Lastly, thanks to my parents for their encouragement and to my wife for her patience and support.

NOMENCLATURE

H_v	Vickers hardness
P	Applied load
d	Indentation diagonal
A_P	Projected cross-sectional contact area
A_S	Actual contact surface area
g	Gravitational acceleration
H_{IT}	Indentation hardness
p_m	Mean contact pressure
C	Constraint factor
E	Elastic modulus of the sample
$E^{/}$	Elastic modulus of the indenter
E^*	Elastic modulus of the sample and the indenter
σ	Hertzian contact stress
a	Contact radius for Hertzian contact stress equation
Y	Compressive yield strength
h_p	Measured depth of penetration
h_r	Residual penetration depth
h_e	Elastic penetration depth
h_a	Upper contact depth from reference datum
h_t	Total penetration depth

A	Actual area of contact
Ai	Ideal area of contact
Δh	Error in the tip displacement measurement from tip rounding
α	Surface roughness
σ_S	Asperity height
R	Indenter radius
a_O	Contact radius obtained under the same load for a smooth surface
ICF	Indentation correlation factor

TABLE OF CONTENTS

CHAPTER Page

LIST OF FIGURES

FIGURE Page

FIGURE Page

LIST OF TABLES

CHAPTER I

INTRODUCTION

The continued research and development of engineering materials is vital for all devices, machines, and structures. A sense of immediacy should be taken since structures continue to fail from fractures, machines persist to fail from excessive wear, and devices continue to fail for many mechanical reasons, including corrosion. Not to focus on corrosion, but a very realistic figure in the $30 billion range has been suggested as the possible savings (annually) if all economical measures were taken to prevent and/or hinder corrosion [1]. However, the cost of material related failures could be orders of magnitude greater than this number, which may be prevented with the benefit of more information. For example, information on the distribution and diffusion of carbon across a weld nugget can provide information necessary to prevent material related failures in gas and oil pipelines. The purpose of this research is to provide the petroleum industry and scientific community with an accurate correlation to determine the Vickers hardness for features too small for conventional macroindentation hardness testing techniques.

Currently, the gas and oil pipelines in the petroleum industry are challenged with material related failures in liquid state fusion pipeline welds located in arctic conditions. These pipelines are made using API 5L X-80 steel, a top candidate in oil and gas field developments due to having a lower cost (as result of thinner wall thickness) and maintaining high strength. However, in the extreme conditions of the arctic, the liquid

---

This thesis follows the style of the Journal of Applied Mechanics.

state fusion welding techniques change the mechanical properties of the X-80 steel upon recrystallization of the weld causing material related failures in the welds.

The focused testing in this research may help determine an alternate pipeline welding technique called friction stir welding (FSW) by providing a correlation that can be used to improve our understanding of microstructural features created by FSW. The microstructural feature in the weld nuggets of X-80 steel is identified as a MA (martensite-austenite) island, which is typically 250-500 nm in length. The challenge facing the petroleum industry and the scientific community is that the hardness of this MA island and other microstructural features cannot be tested exclusively by traditional methods due to the competing size of the macro-scale indenter tips. Therefore, by using the standard nanoindentation test method and applying the correlation recommended, this research will improve the understanding of the MA island and other microstructural features.

For the petroleum industry, if the FSW welding technique is proven to be a substitute for traditional liquid-state fusion welding techniques in extreme conditions, this research would have aided in implementing a welding technique that improves the project economics of developing oil and gas fields. The improved economics are a result of the FSW technique having no consumables, requiring less set-up costs, and creating a lower environmental impact. These factors are in addition to optimizing pipeline up-time as a result of the stronger welds. The improved economics would then support oil and gas field developments, thereby increasing oil and gas supply rates. This boost in

available energy would then offset the cost of gasoline to consumers as a result of enhancing the energy supply.

HARDNESS

Regardless of one's trade, at some point in time people develop their own perception of hardness. A firefighter may think of the hardness of a material in terms of the tool(s) required to remedy a situation based on the material that presents the obstacle (i.e. a steel valve on a hydrant versus a locked window). A dentist may think of hardness by the ease of which a given material can be picked, drilled, or worse for the patient, ground. An engineer evaluates a material's hardness by measuring the penetration depth of a loaded indenter in a controlled environment, and shows particular interest in the material's relative ability to resist deformation. In general, the best definition of hardness is a measure of a material's resistance to permanent deformation or damage caused by a harder material [2].

The measurement of hardness is dependent on what method was used to measure it. In order for the hardness measurements to be comparable, the method of the tests must be followed through in similar conditions. Another important concept is that hardness is not dependent on a single physical property; it is dependent on the elastic and plastic characteristics of the material. As a result, the elastic modulus, yield strength, tensile strength, elasticity, and brittleness influence the measured values. The relation between hardness and strength is the pressure required for plastic deformation to occur. A final important concept is that the hardness property of a material may change during

the test. It is known that during an indention test, the initial penetration produces an increase in the resistance of the material to further indention. This implies that the hardness properties are a function of the crystal structure of the sample material. That is, the configuration of the atoms packed together and their net stability as a structure.

Testing the hardness of a material does not require advanced operator skill; therefore, it is widespread. Most indentation type hardness testing methods are considered to be nondestructive. They are very useful in determining the suitability of certain materials for specific applications. The methods also lend themselves as being a primary choice for testing the uniformity of a product, or determining the level of success that has been achieved by heat treatments or a fabrication method. This is not only because of the ease of conducting the test, but also due to the low relative cost, high repeatability, high reproducibility, and the consistent universal 'language' or standard that the method provides. These characteristics have a great appeal to the engineer interested in hardness values. In this method, the hardness is measured by pressing a hard indenter (of known shape) into a material under standard conditions, leaving a permanent impression.

The different methods of testing hardness can be divided into two categories, static tests and dynamic tests. Since the 1930s, six methods of measuring hardness have become the most distinguished [2]. The first, and the one utilized in this research (at least a variation of it) is the static indentation test. This test is performed by applying a steady load to an indenter (most commonly a diamond pyramid, diamond spheroconical, or a tungsten carbide ball) and then calculating the hardness from the area or depth of the

indentation. A dynamic indentation test occurs when a number of spheres are released from a certain distance above the sample and the hardness is calculated from the indentation size and the energy absorbed from the impact [2]. To continue listing the methods, a third test is known as the rebound test. This is where a weighted sphere or diamond tipped object is released from a fixed height and the hardness is measured from the resulting height of the object's rebound. Similarly, the fourth test is a pendulum recoil test. In this test a steel sphere is attached to a swinging pendulum, and the hardness of the stationary piece is determined from either the amplitude of the first impact or the duration of oscillation of the succeeding swings.

Another common hardness test is the scratch test, which can be divided into two different methods. The first method is a comparison between two materials where the harder material is determined by the material that visibly shows the least severe signs of being scratched by the other. The second scratch test is performed when a scratch is made with a diamond or steel indenter traversing a distance along the material with an applied load (load could be definite or increase with distance) [2]. The hardness is determined by the width and depth of the groove that was formed. The last hardness test method is the abrasion test, which is also considered to determine the materials machinability. There are many variations to this test; however, all of them involve measuring a material's resistance to wear when a sliding, rotating, sanding, or cutting type of operation is applied.

In this research the static indentation test is used to determine the hardness of materials. This method has a broad range of testing conditions. The most common

variants are the indenter tip and the load applied. A tungsten carbide sphere or a diamond cone or pyramid is used to prevent the indenter tip from being damaged by the test piece. This consideration is made because test pieces have unique values in a very broad range of hardnesses.

CHAPTER II

MOTIVATIONS AND OBJECTIVES

The objective of this research is to provide the petroleum industry with an accurate correlation to determine the Vickers hardness for features too small for conventional macroindentation hardness testing techniques. This can be done by testing the feature(s) using a standard nanoindentation technique and then applying the correlation recommended in this thesis to acquire the Vickers hardness values. The correlation is found by analyzing the test data from each test method and developing an expression that relates the two techniques. Another anticipated contribution of this thesis is to provide a research methodology to develop hardness correlations for materials other than metals.

As mentioned above, this thesis serves as a research methodology and computational guide to improve the current understanding of certain microstructural features. Generally, these features may be difficult to test without great optical and mechanical precision. They may also have properties that are not characterized relative to the matrix material. The expectation here is to develop an accurate correlation between the two testing techniques and to apply it successfully under the same conditions, and with the same equipment. The successful outcomes of this research will provide a correlation between the two test methods, and lead to a research methodology for improving our understanding of the hardness of materials at the nano-scale.

The strategies to achieve these objectives are nicely accommodated by the instrument capabilities in the on-campus laboratories. To begin, the Rockwell hardness

test instrument located in the mechanical engineering laboratory will utilize the superficial Rockwell hardness scale and the Brale indenter (spheroconical diamond indenter). The Rockwell test characterizes the hardness of materials from the penetration depth of an indention and displays the values directly without taxing measurement or calculation. The Rockwell and nanoindentation instruments utilize the same indentation measurement technique for determining hardness. Therefore, after converting the Rockwell test results to the Vickers hardness scale according to the ASTM E 140 standard, the values using the two testing techniques should be very comparable (if not off by a common factor). Using the ASTM conversion standard to Vickers hardness scale reduces error introduced when experimentally determining the Vickers hardness. Vickers hardness testing requires optical measurement of the residual indent diagonals that often challenge the operator's measurement skill and introduces errors in the hardness value.

CHAPTER III

MULTI-SCALE INDENTATION TECHNIQUES

This chapter explains the experimental methods used to acquire the test data in this research. Included in the chapter are sections detailing materials selection, macroindentation hardness testing, and nanoindentation hardness testing. The section on nanoindentation hardness testing includes information about nanoindentation test standards, instrument construction, installation, and calibration, and working distance and initial penetration. Also included is background information on indentation hardness and modulus, load-displacement curves, indentation at the nano-scale, and nanoindentation modeling.

MATERIALS SELECTION

The scientific community has developed and commercialized an abundance of metals to choose from, all of which provide a unique set of properties. For instance, carbon and alloy steels do not provide the latitude in heat treating that tool steels do. And neither offer comparable resistance to corrosion initiation quite like stainless steels. The same could be said for cast irons, cast steels, and powder metallurgy materials. Other unique properties come from aluminum and its alloys, copper and copper alloys, magnesium, nickel, refractory metals, titanium, and zinc [3]. However, the materials discussed and evaluated in this research are tantalum and O1 tool steel. Their relevance to this research will become clear in the coming chapters, in addition to the roles that they play in the petroleum industry.

Tantalum was considered for this research mainly because it is pure, noble (with a very thin oxide layer), well characterized, and relatively easy to machine. Although not discussed in this research, when tantalum is mixed with iron it imparts excellent corrosion resistance [4]. As a result, it is used in corrosive environments such as oil and gas pipelines. Other pertinent properties for tantalum are discussed below. Tantalum is classified as a refractory metal (heat resistant metals with melting temperatures over 3000ºF (1650ºC)). It has a density of 0.601 lb/in^3 and a very high melting temperature of 5425ºF (2996ºC); when cold worked it has a hardness of 150 H_v and E of 186 GPa [4,5]. Tantalum is considered to have excellent corrosion resistance, and among refractory metals, have good machinability and good thermal conductivity. Ta is inert to almost all inorganic and organic materials at room temperature with exception to sulfuric and fluoridic acids, hot oxalic acid, and strong alkalies. Like many other metals, tantalum becomes less chemically resistant at elevated temperatures, but it is still better than most stainless steels, titanium, zirconium, and superalloys [5]. Current uses for tantalum include capacitors in electronics, ballistic armor penetration, special chemical vessels, piping, and heat exchangers [6]. Drawbacks to this material are the welding environment requirements and cost. Tantalum metal ingot cost around $320/lb at the end of the year 2006, but having item(s) coated with Ta can mitigate this high cost.

Another material used in this research is O1 tool steel (UNS designation of T31501). Tool steels are used in the petroleum industry for many applications from pipe handling equipment to drill bits. However, the reason for choosing this material in this research is because it offers a broad range of hardness (and therefore applications) and

has well-dispersed very fine carbides that will minimize interference in nanoindentation testing. Tool steel is widely considered to be a carbon or alloy steel that is much more capable of being hardened and tempered. This is because most tool steels have a greater number of alloying elements than alloy steel. Therefore, the greatest factor distinguishing carbon and alloy steel from tool steel is the manufacturing process. This process begins with the way that the steel is melted and/or re-melted. These techniques determine the purity of the steels and allow particular control of alloying that is not easily obtainable with the most commonly used carbon and alloy steels. Additionally, tool steel is made in smaller lots and must conform to certain quality requirements in order to give specific properties. Other factors that distinguish tool steel from carbon and alloy steel are that tool steels cost more, have better hardening ability, are easier to heat treat, are generally more difficult to machine, and many have better heat resistance. Tool steels also have high tempering temperatures, which allow them more resistance to thermal softening effects [5].

Throughout this research, it was found that tool steels have been developed and enhanced for nearly ninety years. Over this period there have been around seventy types of tool steels developed (due to various needs). From the numerous types of tool steels only a couple dozen are readily available, and only half a dozen of those are typically stocked by designers and metallurgists. Tool steels have a prefix letter identification system to represent the category that the material will be used in. The four major categories are cold work, hot work, shock resisting, and high speed. Type O1 is in the cold work category. As mentioned earlier, the chemical composition of most tool steels

are different from alloy steels. There are a larger number of alloying elements in tool steels that account for their different properties. Besides iron and carbon and the elements listed in Table 1, additional alloying elements in tool steels may include molybdenum, nickel, and cobalt. An important aspect regarding tool steel is that the additional alloys do not pass on any corrosion resistant properties to the steel. This happens as a result of the alloying elements combining with carbon to form carbides. Although some grades have as much chromium as stainless steels, the alloy does not go into solid solution to form a passive layer on the surface [5].

The existence of the alloy carbides in the microstructure of the tool steel is also a differentiating factor from other steels. The carbide phases are chromium, molybdenum, tungsten, and/or vanadium carbides [5]. These carbides are harder than their martensitic matrix. Some tool steels (like cold-work and high-speed tool steel) have larger carbides than others. These larger carbides allow tool steels to have significantly greater abrasion resistant properties than carbon and alloy steels. More carbides in the microstructure give greater abrasion resistance, and larger carbides provide more resistance than smaller ones. However, tool steels that have similar compositions to alloy steels contain carbides that are too fine to be seen in an optical microscope at less than 400 magnification. This gives way to the next statement. Although the shape of the carbides may fluctuate, the volume fraction of the carbides will increase with increasing carbon content [5].

O1 tool steel is important not only because it has well-dispersed, very fine carbides that will minimize interference in nanoindentation testing, it is also the most widely used alloy of the oil-hardened grades. Type 01 is often a first choice because it

machines easier than other tool steels and cold worked steels. Three other popular grades are the O2, O6, and O7. These steels contain 2-3% of very fine carbides (a relatively small volume fraction). The carbides present are mostly Fe_3C type with hardness less than 1000 kg/mm^2 [5]. The ASTM A681 - 07 manufacturing requirements are listed in Table 1 below. The remainder of the composition aside from the requirements listed below is iron.

Table 1. O1 tool steel chemical composition requirements min./max. (%) [7].

C	Mn	P (max)	S (max)	Si	Cr	V	W
0.85/1.00	1.00/1.40	0.030	0.030	0.10/0.50	0.40/0.70	0.00/0.30	0.40/0.60

01 tool steel has a density of 0.283 lb/in^3 and a melting temperature of 2590ºF (1421ºC); when cold worked to 535 H_v it has an E of 217 GPa [4,5]. These considerations, as well as the information given in the first column in Figure 1, helped determine the O1 steel as the best candidate for this research.

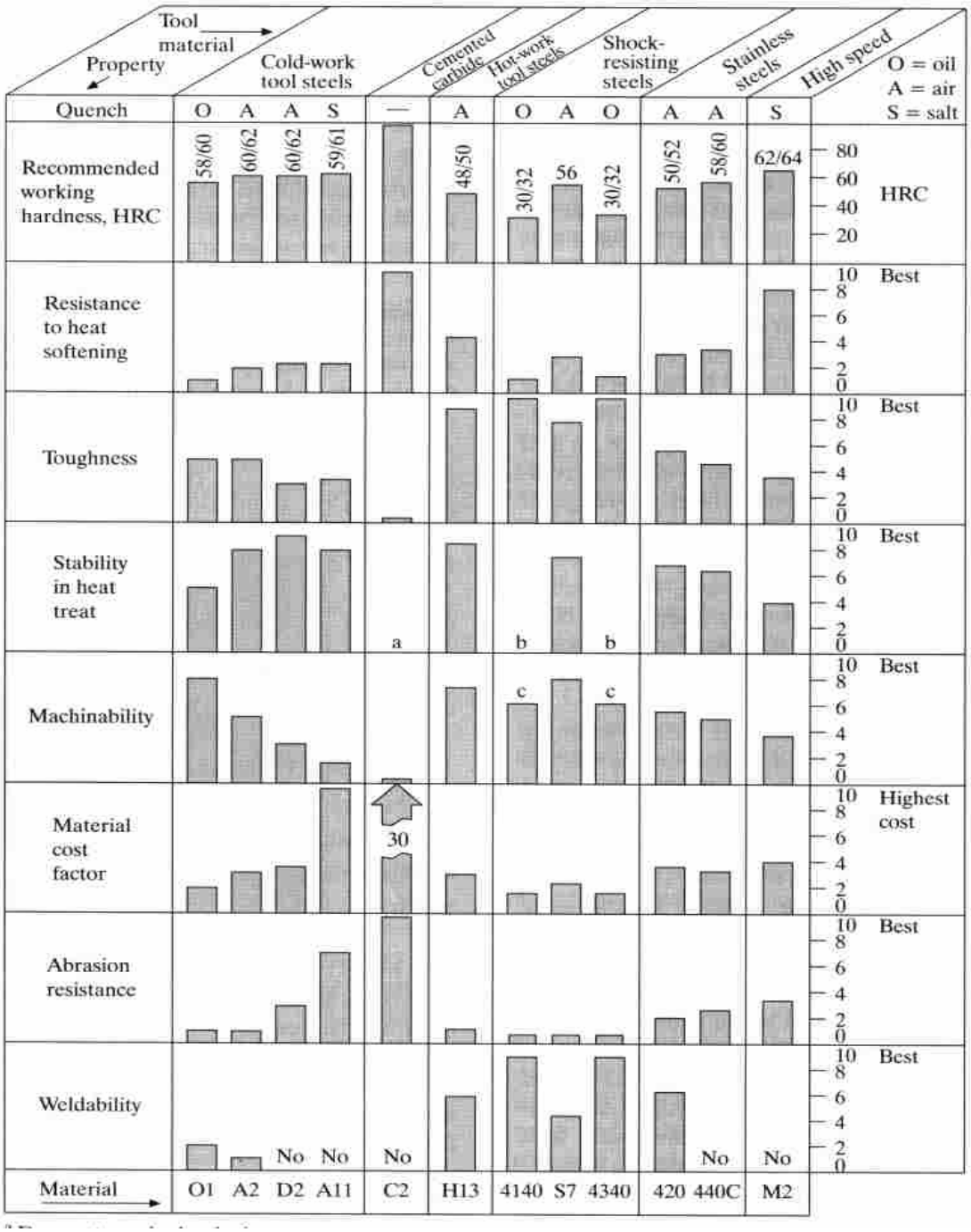

Figure 1. A comparison of various tool steel properties at a specific working hardness [5].

MACROINDENTATION HARDNESS TESTING

The macroindentation hardness testing method used in this research is the well-known Rockwell hardness test. This test determines the hardness of materials using the indentation penetration depth of an indenter and compares it to that of a reference material. The correct notation for a Rockwell hardness value is HR followed by the scale (e.g. 56 HRC) where C is the letter for the scale used. Table 2 lists all currently used Rockwell hardness scales.

Table 2. Rockwell hardness scales [8].

Scale Symbol	Indenter	Total Test Force, kgf
B	1/16-in. (1.588-mm) ball	100
C	diamond	150
A	diamond	60
D	diamond	100
E	1/8-in. (3.175-mm) ball	100
F	1/16-in. (1.588-mm) ball	60
G	1/16-in. (1.588-mm) ball	150
H	1/8-in. (3.175-mm) ball	60
K	1/8-in. (3.175-mm) ball	150
L	1/4-in. (6.350-mm) ball	60
M	1/4-in. (6.350-mm) ball	100
P	1/4-in. (6.350-mm) ball	150
R	1/2-in. (12.70-mm) ball	60
S	1/2-in. (12.70-mm) ball	100
V	1/2-in. (12.70-mm) ball	150

There is also a superficial Rockwell hardness scale. The difference between this and other common Rockwell hardness scales is that the minor and final test forces applied during testing are much lower. These lower test forces involve a lower penetration depth scale. Table 3 lists the test forces and scales.

Table 3. Superficial Rockwell hardness scales [8].

Total Test Force, kgf (N)	N Scale, Diamond Indenter
15 (147)	15N
30 (294)	30N
45 (441)	45N

This scale is used on brittle and very thin materials and utilizes the diamond spheroconical Brale indenter. The Brale indenter has a 120° ± 0.35° included angle. The tip of the diamond is spherical with a mean radius of 0.200 mm ± 0.010 mm. Figure 2 illustrates these features.

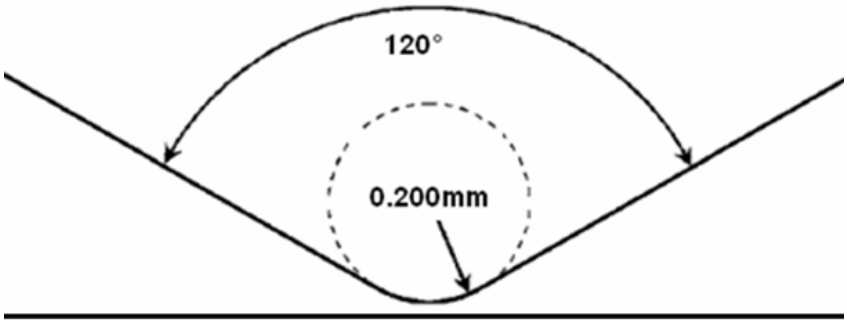

Figure 2. Profile of Brale spheroconical diamond indenter tip.

The method for calculating the Rockwell hardness number is also important. A short description of the test procedure is explained first. The Rockwell test is administered by applying the predetermined minor force to the sample, increasing to the predetermined total test force, and returning to the minor test force. The difference of the two penetration depth measurements under the minor test force is measurement *h* in mm.

Using measurement *h*, the Rockwell hardness and superficial Rockwell hardness is calculated from the equations below.

$$HR = 100 - \frac{h}{0.002} \tag{3.1}$$

$$Superficial\ HR = 100 - \frac{h}{0.001} \tag{3.2}$$

In order to compare the macroindentation test data to the nanoindentation test data, the superficial Rockwell hardness values will be converted to the Vickers hardness scale according to ASTM E 140. As a note, the Vickers indenter used in the Vickers test has four sides, each having an included angle between opposite faces of 136º. The loads used in the Vickers test typically range from 1 to 120 kg. Traditionally, when the load is removed, the diagonals of the indention are measured optically. What will become more pertinent later is that the Vickers hardness number (H_v) is given by the ratio of the load to the cross-sectional contact area of the indention in kg/mm^2. The shape resulting from a Vickers indentation is determined by the amount of elastic recovery, and if piling-up or sinking-in occurred (discussed in greater detail in Chapter VI). The Vickers hardness number is calculated from the simplified equation below.

$$H_v = \frac{2P\sin 68^\circ}{d^2} = \frac{1.8544P}{d^2} \tag{3.3}$$

In the equation above, H_v (kg/mm^2) is the Vickers hardness, *P* (*kg*) is the test force, and *d* (*mm*) is the diagonal of the indentation. Since the geometry of the indention made with the Vickers pyramid is independent of the depth (and therefore the load), the hardness should then be independent of the load [2].

Many experts would agree that the greatest challenge for successful measurements with the traditional Vickers test machine is the skill of the operator and the positioning of the indention. Using the previously discussed conversion strategy and the macroindentation hardness testing machine used in this research, such challenges will not be a factor. Shown in Figure 3 below, the machine used is the Instron Series 2000 Rockwell® using standard Wilson test blocks, penetrators, and calibration sets. The tester conforms to ASTM E 18, and ISO 6508 (among others). The tester also automatically converts to other hardness scales and values according to ASTM E 140 or DIN-50. In order to help avoid errors the instrument has a load cell fixed to the indenter and electronic closed-loop control [9].

Figure 3. Instron Series 2000 Rockwell® hardness tester with Wilson test block and penetrator.

Instron's software provides charts and outputs including individual test results, regression and correlation, histograms, normality test, and statistics. The test forces are controlled by the same software, which ensures precision and repeatability. As discussed above Rockwell hardness values are measured from the penetration depth into the material. Therefore, this instrument will yield excellent results due to its great precision and resolution. A final specification pertinent to this research is the instrument's guaranteed gage repeatability and reproducibility (GR & R) of 5% or less [9].

NANOINDENTATION HARDNESS TESTING

Nanoindentation is a modern area of materials hardness testing that is very useful in the mechanical engineering field. The concept of the test is rooted in materials research. Currently there is a need for more information associated with this method. Nanoindentation is a test where the penetration depth of the indentation is on the order of 10^{-9} m, or nanometers. The most common length scales in conventional hardness tests have penetration depths measured on the order of 10^{-6} m (microns) and 10^{-3} m (millimeters).

Another unique property of the nanoindentation method is the measurement mechanism used to determine the hardness. As mentioned earlier the Vickers static indentation test calculates the hardness from the area of the indentation, which is determined from direct measurements of the dimensions of the impression in the material after removing the indenter/load. The size of the indention in nanoindentation testing is too small to accurately measure directly. The contact area is calculated using

the penetration depth into the sample and the known geometry of the indenter. Therefore, the cross-sectional area of contact between the sample and the indenter at any applied force can be calculated (measured indirectly).

The applied loads are typically in micronewtons with nanonewton resolution/increments. The fundamental goal of the test is to acquire the hardness of the sample and its elastic modulus from measurements of penetration depth and indenter load [9]. The procedure used to process the acquired data is a major component of the accuracy and quality of the results. The analysis in this research not only extracts the material properties listed above, but it is also cognizant of and recognizes incorrect or insufficient data that causes errors.

The hardness and elastic modulus aren't the only parameters determined by nanoindentation testing. Others include the strain hardening exponent, fracture toughness, cracking, phase transformation, energy absorption, creep, and viscoelastic properties [10]. Because this amount of information can be gleaned from the method, nanoindentation is becoming more popular in industry. Now to explain how the fundamental goal is achieved. When the indenter makes contact with a sample with a steadily increasing load, the penetration depth and load are recorded. This takes place at each load increment, providing a measurement of hardness as a function of penetration depth below the surface. This behavior is shown in the load-displacement curve in Figure 4(b).

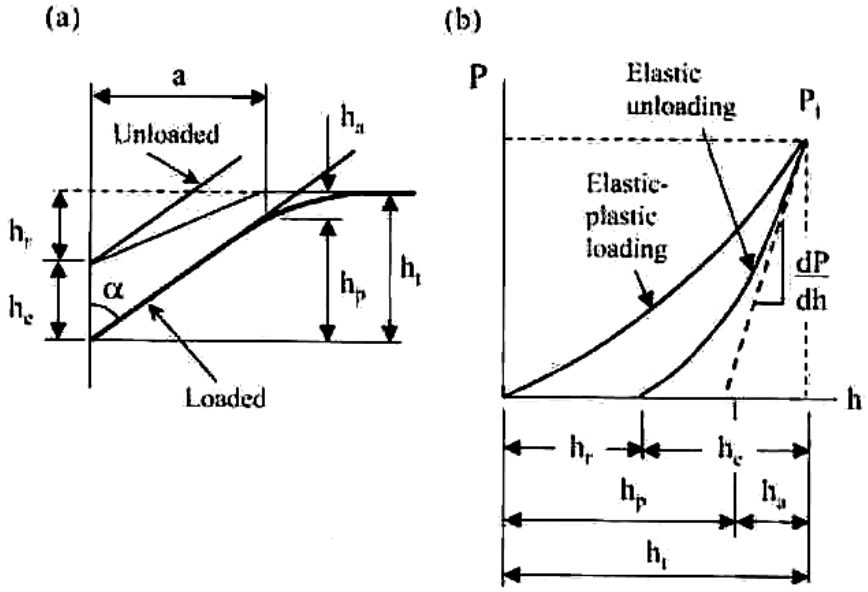

Figure 4. Typical schematics for a conical indenter. Part (a) illustrates a profile of the indentation parameters. Part (b) illustrates a load-displacement curve [10].

The final penetration depth is recorded when the maximum load is achieved (prescribed in the test design). Then the load is progressively removed and the penetration depth is recorded at each load increment. The structural response during the loading/indentation cycle is typically elastic at initial contact. With progressive loading, the response is followed by yielding within the sample and plastic deformation. Plastic deformation typically occurs from one of two mechanisms. The first is from slip planes, and the second is from twinning (shearing of a given plane). Assuming that yielding has taken place, the load-displacement curve will follow a different path during the unloading/retracting cycle until the load is completely removed. As a result of these actions, an impression is left in the sample. The dashed line in Figure 4(b) shows how the elastic modulus is determined (the slope of the tangent to the unloading curve

originating from maximum force). During this type of test, a brittle sample may develop fine cracks, especially if using a pyramid-shaped indenter such as the three-sided Berkovich indenter or the four-sided Vickers indenter. The cracks usually begin at the corners of the indentation impression and are used to calculate the fracture toughness of the sample [10].

Nanoindentation is often chosen over the macro-scale tests because of its higher measurement accuracy by virtue of its length scale. Since being standardized in June 2000, ISO 14577-1 to -4 (explained below) advanced from being introduced into industry to becoming common. The nanoindenter used in this research is operated by computer control and does not require vacuum chambers or other laboratory infrastructure. Figure 5 below shows the nanoindenter installed with the environmental cover. The current development of the nanoindentation technique makes it useful to evaluate new materials by both academic and industrial research laboratories [10].

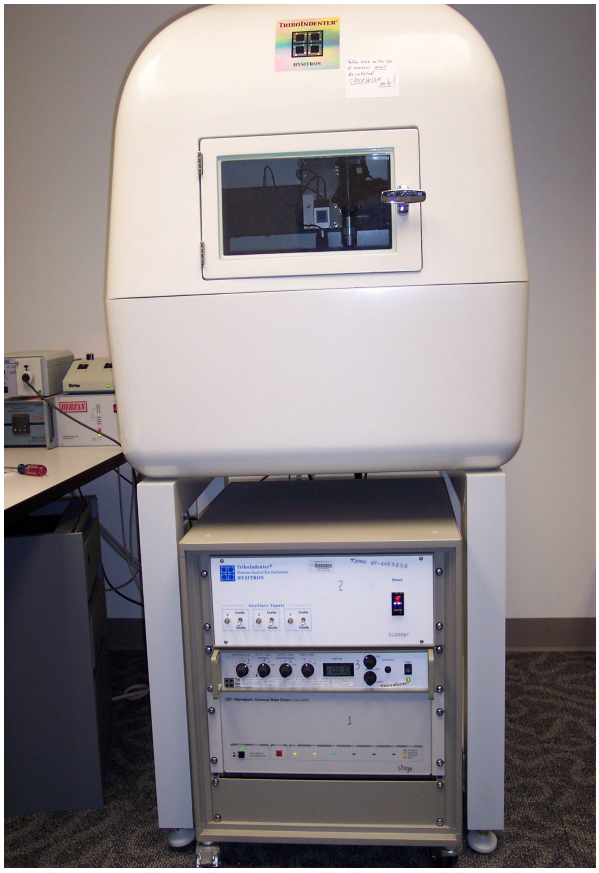

Figure 5. Hysitron's TriboIndenter nanoindenter with environmental cover.

Nanoindentation Test Standards

The test standard for nanoindentation testing is the ISO 14577. It is titled "Metallic materials - Instrumented indentation test for hardness and materials parameters." It is explained in the test standard that Brinell, Rockwell, and Vickers test results give hardness values once the load is removed. As a result, the elastic deformation is not evaluated [11]. The ISO 14577 standard allows the evaluation of materials using force and displacement during elastic and plastic deformation. In addition to determining traditional hardness values, the properties mentioned earlier can be determined using this standard. ISO 14577-1 specifies the method of indentation test

for determining the hardness and other material parameters for the three ranges given in Table 4 [11].

Table 4. Hardness testing ranges defined by ISO 14577-1 [11].

Macro Range	Micro Range	Nano Range
$2\ N \leq F \leq 30\ kN$	$F < 2\ N\ ;\ h > 0.2\ \mu m$	$h \leq 0.2\ \mu m$

Many of the specifications in the ISO 14577-1 standard were/are listed in this manuscript; however, the following paragraphs serve as a summary.

The governing parameters of the test can be controlled by force or displacement. The applied force, penetration depth, and time are recorded during the test. The applied force and penetration resulting from the test is a function of time, thereby producing a loading rate. The instrument has the capability of applying predetermined test forces within the desired load settings and implements them according to ISO 14577-2 standards. The instrument also compensates for the machine compliance and determines the correct tip area using the appropriate indenter area function [11].

The test should be performed on a region of the sample surface that allows the determination of properties within a reasonable amount of uncertainty. The contact area should be clean, dry, and at an ambient temperature between 10°C and 35°C. However, the stability of the temperature during a test is more important than the ambient temperature. The recommended conditions are 23°C and less than 50% relative humidity for testing in the nano and macro ranges [11].

The standard also provides useful information summarized below. The test piece should be firmly supported for machine compliance reductions. The reference datum for the indentation should be determined individually for each dataset. The time segments for the test should be noted in order to obtain comparable test results. The test force should be applied with the least amount of shock or vibration. When determining the reference datum, the approach speed of the indenter in the working distance should be low in order to prevent changing the mechanical properties as a result of the impact. Typical approach rates are between 10 nm/s and 20 nm/s [11].

The uncertainty of the test results comes from a combination of uncertainties from several sources. These can be separated into the two categories shown in Table 5.

Table 5. Sources of uncertainties by function [11].

Type A: Measurements related	Type B: Equipment related
Reference datum	Applied force and Displacement
Force and displacement measurements	Instrument compliance
Fitting a tangent to the unloading curve	Area function calibration
Thermal drift rate	Thermal drift calibration
Projected contact area	Tilt of test surface

The test standard also specifies what a report of the test should include. The first thing is to reference the ISO 14577-1 standard. The report should also include all details necessary for identifying the test piece, the material and shape of the indenter, where the

test piece was tested, and the detailed area function of the indenter. Another part to include is the testing cycle (control method and full description of the cycle profile), which includes set point values, rates and times of force or displacement, position and length of hold points, and the number of points logged for each section of the cycle. The standard also suggests including the results obtained, the total expanded uncertainty, the number of tests, and the method applied for determining the reference datum. Some final mentionables were the details of any occurrence that affected the results, the temperature of the test, date and time of test, and analysis methods [11].

The ISO 14577-1 standard also gives the method used in determining the nanoindentation hardness. This is shown in Chapter VII, equations (7.6-7.8).
As mentioned above, the indentation modulus is calculated from the unloading curve and is comparable with the Young's modulus of the material. There can be differences in the two moduli if either pile-up or sink-in occurs. The standard also briefly describes the effects of machine compliance, indenter area function, and the influence of the sample's surface roughness on the accuracy of the results [11].

The last section of the ISO 14577-1 standard provides a correlation between nanoindentation hardness values and Vickers hardness values. The nanoindentation hardness may be correlated to Vickers hardness for a wide range of materials using the scaling function outlined in the standard. The standard provides a scaling function based on the Vickers indenter where the projected area function is known. Therefore, nanoindentation hardness measurements are related to the Vickers hardness values by

this scaling factor. This is determined by defining the Vickers hardness equation first and then substituting equation (3.4) to yield the scaling factor for the Berkovich indenter.

$$H_v = \frac{P * A_P}{A_P * A_S * g} \tag{3.4}$$

where A_P is the cross-sectional area of the contact between the sample and the indenter, A_S is the surface area of the indenter in contact with the sample, and g is the gravitational acceleration. Now the ratio of the projected area to the surface area for any distance from the tip of the Berkovich indenter is needed.

$$\frac{A_P}{A_S} = \frac{24.50}{26.97} = 0.9084$$

Substituting equation (3.4) and reducing gives the expression below.

$$H_v = \frac{H_{IT} * A_P}{g * A_S} = 0.0926 * H_{IT} \tag{3.5}$$

However, the ideal geometry for a Berkovich indenter tip is not typically achieved at penetration depths less than 6 μm, causing the scaling function to be inaccurate within this penetration depth [11]. This specification creates a need for interpretation of test data at shallower depths in standard hardness scales. The penetration depths achieved in this research average 200 nm.

As discussed, ISO 14577-1 specifies the indentation test method for determining material hardness (among other material properties). However, ISO 14577-2 specifies the method of verification and calibration of the instrument for performing the indentation test in accordance with ISO 14577-1. Moreover, it describes a direct verification method for checking the main functions of the instrument and an indirect

verification method for determining the repeatability of the instrument. Both methods are used for routine confirmation of the instrument in service [11].

The direct verification should be performed at 23°C ± 5°C. The instruments used for verification and calibration should be acknowledged by national standards. The direct verification involves verification of the indenter, the indenter area function, and the testing cycle. The direct calibration involves calibration of the test force, the displacement, and the machine compliance [11].

The indirect verification should be performed periodically or before tests requiring high accuracy. If the testing machine is used in the nano range, it is recommended to perform the indirect verification more frequently. The indirect verification should be performed at 23°C ± 5°C using reference blocks calibrated in accordance with ISO 14577-3. These reference blocks can be calibrated for hardness, indentation modulus, and other mechanical properties. The indirect verification should be performed for at least two test forces frequently used. Verification of the area function for tests with penetration depths less than 6 μm also benefits from this verification. It is recommended that two reference blocks covering a wide hardness range be chosen [11].

ISO 14577-3 specifies a method for the calibration of reference blocks used for the indirect verification of instruments for the indentation test that was specified in ISO 14577-2. The blocks should be as homogenous and stable as possible. They should also be greater than or equal to 2 mm thick for the nano range, demagnetized, free from

scratches, and within the tilt limits specified in ISO 14577-1. It may be necessary to polish the surface prior to using the block in the nano range [11].

ISO 14577-4 provides guidelines for conditions where the hardness measurement is/is not influenced by the substrate of a coating. Where the measurements are influenced by the substrate, the standard provides analytical methods to enable the coating properties to be extracted from the composite measurement. The extent to which a coated component can withstand an external applied force is an important property. Coatings are applied to provide wear resistance that is usually enabled by their hardness. The elastic and plastic properties of a coating determine its performance [11].

Instrument Construction, Installation, and Calibration

The nanoindentation instrument used in this research is the Hysitron TriboIndenter®. This instrument is a fully automated, multi-load range indentation and scratch test system. In addition to determining the hardness and elastic modulus, the instrument can determine the viscoelastic properties of materials. The TriboIndenter® has highly quantitative testing capabilities with indentation and scratch load configurations. Although not fully utilized in this research, the machine is automated with high-throughput capabilities via a staging system that accommodates the samples of different types and sizes. Figure 6 below shows the stage used.

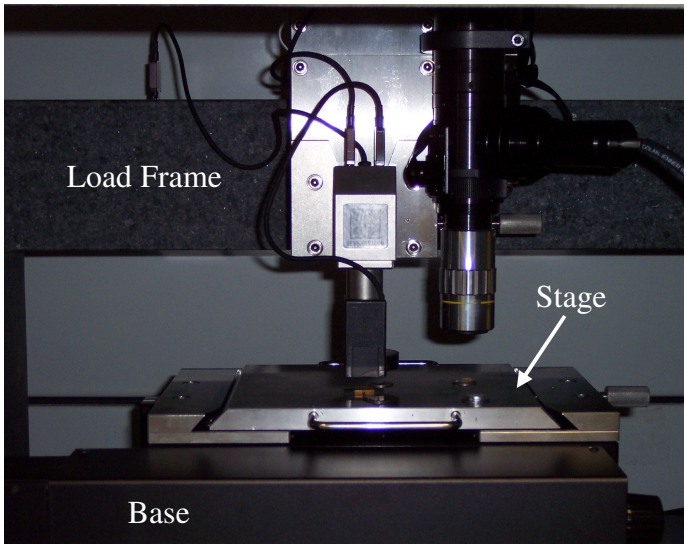

Figure 6. The stage of the Hysitron TriboIndenter®.

The actuation of force and displacement for the instrument is provided simultaneously from a transducer that is based on a 3-plate capacitor technology. The instrument in this research is equipped with a piezoelectric scanner that allows very precise X, Y, and Z positioning of the indenter. In the low load setting of the indenter, the range of force measurement is 1 nanonewton to 30 micronewtons. The displacement resolution is as low as 0.0002 nm. The high resolution is required for indentations made on very small features such as grains or conductive pads [10].

As seen in Figure 5, the environmental enclosure is installed and was utilized during testing. The primary purpose of the enclosure is to reduce thermal and electrical interference as much as possible. The indenter is also safeguarded as much as feasibly possible against temperature variation, vibration, and acoustic noise. Also shown in Figure 6 is the loading frame and base of the indenter. They are constructed from heavy materials in order to reduce transmitting vibration and to minimize the effect of reaction

forces on the displacement readings (discussed as compliance in Chapter VI). In operation, the indenter is given a maximum command force that is applied and the resulting displacement is measured [10].

Many intricate and highly sensitive components of the nanoindenter require calibration prior to use. Thus, prior to testing the materials with this instrument there is an elaborate calibration process that requires approximately two hours. The first component to be calibrated is the transducer (necessary before every experiment). The transducer is used to measure the force applied to the sample. No material is actually penetrated in this process. The indenter tip assembly hovers above the stage and performs a mock indention. The results are recorded and plotted in a force-displacement curve that is ideally flat, starting from the origin. If it is not, the transducer settings must be zeroed out and the process repeated in order to achieve the ideal curve. If this step is eliminated, the force measurements will be inaccurate, therefore, giving inaccurate hardness measurements.

The next component to be calibrated is the optical microscope (shown in action in Figure 7 below). This calibration allows very accurate placement of the indenter (via the microscope) in case there is a specific feature on the material that requires testing. The operator locates the center of a pattern of indents (created by the instrument), which completes the calibration of the optical microscope. This is done in order to synchronize the optical microscope with the indenter tip.

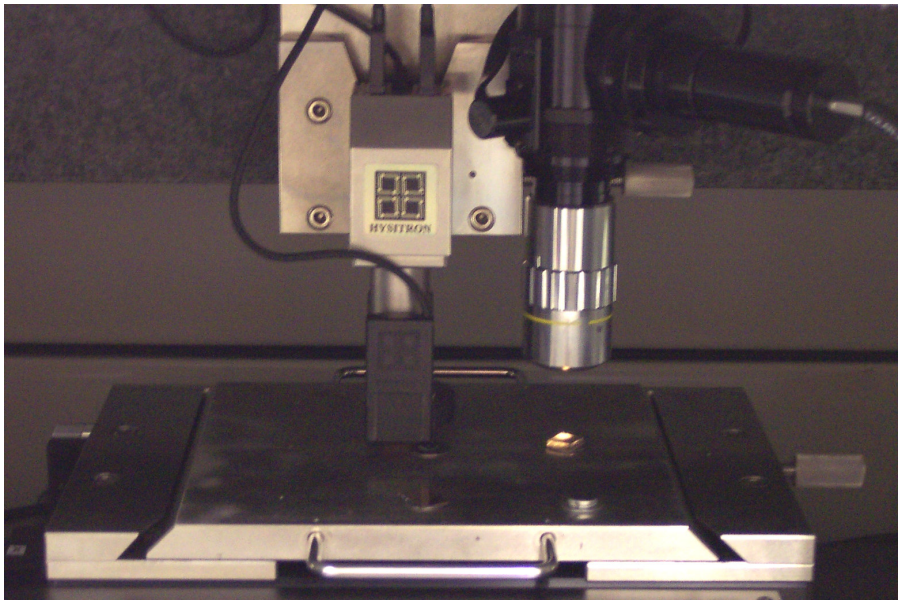

Figure 7. Performing calibrations on test blocks.

The final component to calibrate or develop before beginning the experiment is the indenter tip-area. Although this calibration is the most time consuming, it is critical in determining accurate hardness measurements. Essentially, this exercise accounts for geometrical aberrations from the ideal profile of the indenter tip and creates a depth-area function for the indenter tip. This calibration was completed using a 5-by-5 matrix totaling 25 indents set to penetrate at different depths on a standard fused quartz sample. The result was a plot of the calculated area versus penetration depth. A curve was then fitted using the fifth-order polynomial, shown in the equation below [12].

$$A_P = 24.5h_p^2 + C_1h_p + C_2h_p^{1/2} + C_3h_p^{1/4} + C_4h_p^{1/8} + C_5h_p^{1/16} \qquad (3.6)$$

Each of the five area function coefficients was then entered into the area function of the instrument. This topic is identified and discussed in Chapter VI as a major factor

influencing the hardness measurements. Figure 8 serves as an example of the fitted area function used in this research.

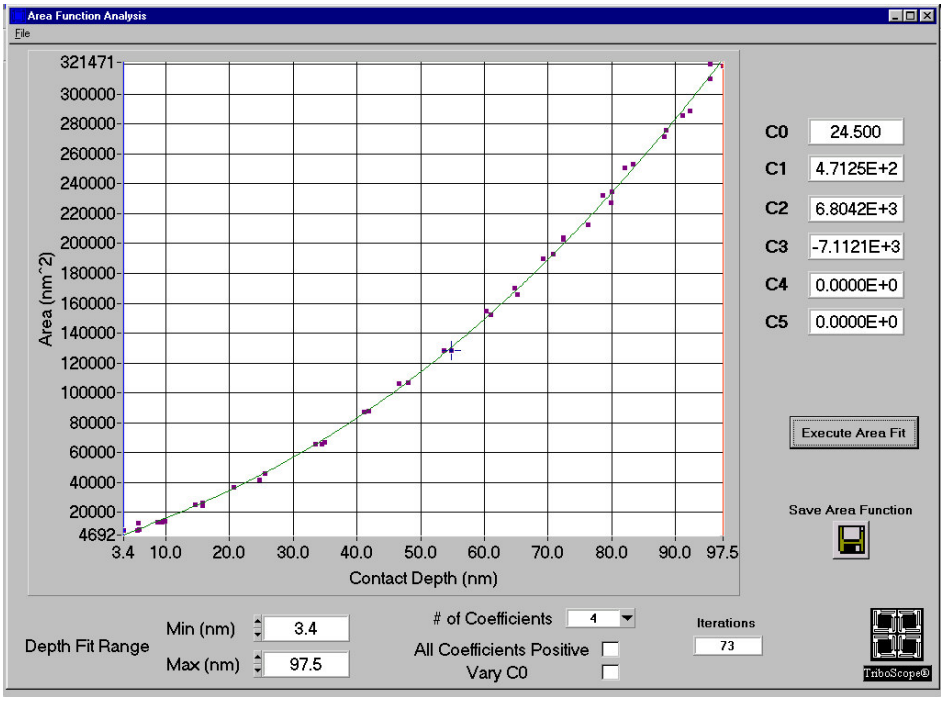

Figure 8. Example of fitted area function [12].

Working Distance and Initial Penetration

The Hysitron TriboIndenter® used in this research has a limited range of displacement over which the indentation depth may be measured. One pitfall to this feature is that this range can be consumed when bringing the indenter into contact with the surface. It then becomes critical that the full range of the depth measurement system is available for measuring penetration depth into the specimen. To do this correctly, the indenter is toggled downward in coarse steps until it is within 1 mm. of the sample surface. Once completed, the new distance is called the working range. These steps

ensure that high-resolution displacement is available for the final approach to the surface and the indention [10].

In this research the surface being tested is as flat as feasibly possible to the surface that it rests on. As disclosed in Chapter IV, the average surface roughness was measured to be in the nano-scale. The importance of these specifications is presented when the reference datum for the sample is determined. Regardless of tilt and average surface roughness, the reference datum determined for a particular sample becomes the reference datum for all of the indentions made on that sample, at that time. This is a consequence of the instrument conducting the test under load control instead of displacement control. The reference datum is chosen when the working distance is established and the indenter makes first contact with the sample. The initial contact should be performed with the smallest contact force possible. Moreover, no matter how small the contact force is, it will result in some penetration into the sample's surface that has to be accounted for in the analysis. More specifically, the initial penetration depth will offset all subsequent displacement measurements taken from this datum. Therefore, the initial penetration depth is added to all displacement measurements to account for this. The instrument used in this research brings the indenter down at a certain velocity (determined by load settings) until the initial contact is made. Initial contact is realized when preset initial contact force is measured. An initial contact force of less than 1 μN is normally used [10].

Indentation Hardness and Modulus

Although the nanoindenter conveniently gives the hardness number, a short explanation is needed concerning how the hardness is calculated. As discussed on page 80 of Chapter VII, the mean contact pressure (p_m) is found by the quotient of the load and the projected contact area. The mean contact pressure is the pressure at the point when increasing the load does not change this value. If it is found in a fully developed plastic zone, p_m represents the nanoindentation hardness (H_{IT}) of the sample at that given load. If a rigid plastic solid exhibits minimal elastic recovery from the material, the mean contact pressure in the fully developed plastic zone is a true representation of the resistance of the material to permanent deformation [10].

Likewise with the hardness, a short explanation is needed concerning the elastic modulus. If it is determined in the manner explained earlier in the Nanoindentation Hardness Testing section, the modulus is formally called the indentation modulus (E_{IT}). Ideally, the indentation modulus is considered to have the same meaning as the term elastic modulus or yield modulus. However, this may not be true for some materials because the measured indentation modulus may be affected by material piling-up or sinking-in. This data becomes an anomaly if it is not accounted for in the analysis of load-displacement data. Therefore, if different testing techniques are used, or if different types of the same material are tested, the resulting moduli must be compared carefully. As discussed in greater detail in Chapter VI, piling-up of material occurs when the work hardening of a material is low, causing the displaced material to flow upwards along the faces of the indenter. An annealed material with a high work-hardening capacity will be

pushed down by the indenter. The sample material in contact with the indenter will sink below the original plane of the surface and the impression will have a concave profile, a phenomenon termed sinking-in [2,10].

Load-Displacement Curves

As mentioned earlier, the objective in nanoindentation testing is to determine the hardness and elastic modulus of a sample from the data acquired. Usually an indention is made in the sample as the load is applied from zero to some maximum and back to zero. Once the load has returned to zero or is removed, the sample tries to restore itself to its original shape. This is usually prevented because of the plastic deformation endured, but there is some amount of recovery due to the relaxation of elastic strains within the material. A common set of curves from the test is shown in Figure 9 below [10].

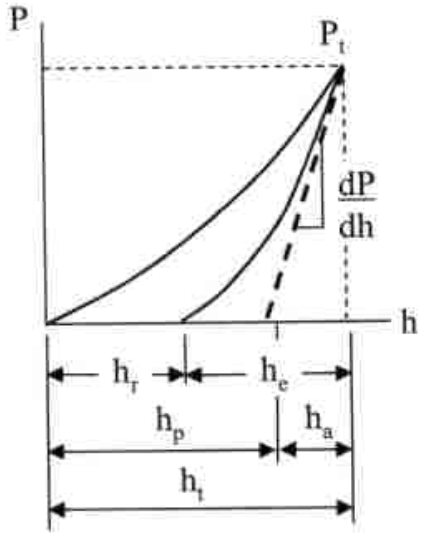

Figure 9. Loading and unloading curve from a typical nanoindentation experiment [10].

Indentation at the Nano-Scale

As thin films were reserving a spot on the podium of technological innovations, knowledge of thin-film mechanical properties became more important. This is the original reason for growth in nanoindentation testing. In order to prevent hardness measurements from being tainted by the effects of the substrate, penetration depths had to be limited to around 10% of the film thickness [10]. Microindentation hardness testing instruments could not apply small enough forces to meet this standard. When they finally could, the size of the indentations could not be determined accurately enough to yield good results [10]. A recent study has found that the material hardness can be measured using nanoindentation and microindentation if the thickness of the film is at least 10 μm [13].

Chronologically, nanoindentation hardness testing became known as depth-sensing indentation testing. This resulted because, as mentioned above, the indenter's penetration depth and geometry were known and used to determine the contact area. In order for this to work, the depth measurement system needs to be referenced to the sample's surface. With the nanoindenter used in this research, the datum is found by contacting the surface with the slightest initial contact force. However, this results in an initial penetration of the surface. This initial contact made by the indenter is accounted for in the analysis. This is not the only correction needed for nanoindentation hardness analysis. Other corrections include irregularities in the shape of the indenter, deflection of the loading frame, deflection of mounting adhesive, and piling-up of material around the indenter. When determining the hardness and modulus of the sample, the influence

that these effects contribute can become as large as the influence of material defects like dislocations and grain sizes [10].

Nanoindentation Modeling

An important tool in understanding the deviations given in test data is computer simulation of the load-displacement curve. This work allows recognition and understanding of deviations by comparing the simulation results with actual events during nanoindentation like cracking or phase changes. Analysis provided by software is valuable because it provides information about the stress states within the sample during the loading and unloading process. Based on the quality of the data and the correlation in this research, an FEA simulation of the process is not necessary in order to understand the localized effects or reconcile differences in the test data and the simulation.

However, a different kind of model is utilized in this research. This model uses a strain gradient plasticity theory to qualitatively explain the most apparent phenomenon in nanoindentation testing, indention size effects (ISE). Although explained in more detail later, ISE are observed increases in indentation hardness when reducing the penetration depth. The strain gradient plasticity theory used to explain ISE in this research is the Nix and Gao model of mechanism-based strain gradient (MSG). Summarized, this model suggests circular loops of geometrically necessary dislocations (GND) with Burgers vectors perpendicular to the sample surface account for ISE and bi-linear behavior. The circular loops or dislocation loops accommodate/interact with the indentation throughout all elastic and plastic deformations. An illustration of this model

is shown in Figure 10 below. Although not discussed here, expressions have been derived to quantify the depth dependence of hardness. In all, the expressions (in addition to other successful theories) predict that the hardness squared is linearly related to the reciprocal of the indentation depth. Such plots are useful in determining bilinear behavior, which is also not discussed here [14].

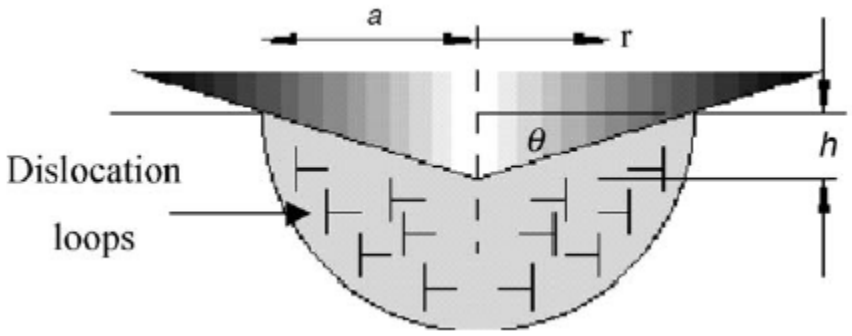

Figure 10. GND loops for ISE modeling [14].

Figure 11 is another illustration of the physical meaning of the theory by comparing the abundance of dislocation sources. This figure allows a clear explanation for the material behavior by illustrating the limited number of dislocation sources.

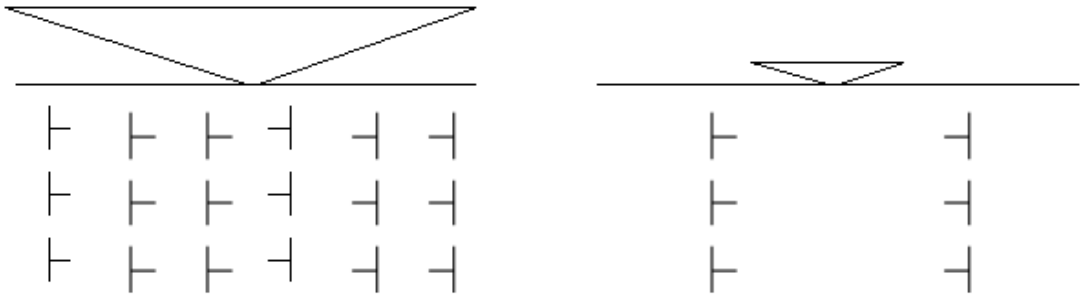

Figure 11. Illustration of dislocation sources for indentation (respectively).

The right side of the figure above shows that at the smaller scale, the population of dislocations become much more scarce. Actually, it was found that the GND density increases with decreasing indentation depth. The increased density of the dislocations is responsible for the increased hardness and ISE in nanoindentation testing [15].

CHAPTER IV

MATERIALS PREPARATION

SAMPLE PREPARATION OF HEAT TREATED SAMPLES

Two O1 tool steel samples in this research were heat treated. They were originally supplied in the annealed condition around 232 H_v. The intent of supplying the material in this condition was for the ease of machining the material. The samples were taken from a 1-inch diameter by 12-inch long rod. In the supplied condition the alloying material takes the form of alloy carbides that are well dispersed in the softer steel matrix. The goal for these two samples was to have one heat treated to around 400 H_v and another around 600 H_v since a third sample can be cut from the rod at about 232 H_v. The heat treatments were intended to change the distribution of carbides and harden the softer steel matrix. There are a few steps in the process, which are designed to achieve the hardness as uniformly as possible. Heat treating was not a significant contributor to the cost of the final product, but was the most influential in the performance of the material.

The first step in the heat treating process was to preheat the samples. One reason for this step was to prevent the samples from cracking as a result of thermal shock. This occurs from heating the material from room temperature to austenitizing temperature in seconds. The main reason for preheating is to ensure a uniform transition to the austenite microstructure. This involves a change in density and volume as the microstructure changes in response to the temperature. The uniform transition was important in order to avoid distortion in the samples. The samples were preheated for 30 minutes at 1300℉

(below the materials' transformation temperature) in order to ensure that the samples were uniform in temperature across their section.

The next step in the process is to heat the samples up to their austenitizing temperature. The austenitizing temperature for O1 tool steel is between 1450℉ and 1500℉ depending on the steel's exact composition. As mentioned before, the alloying material takes the form of alloy carbides diffused in the annealed steel matrix. A higher austenitizing temperature will allow more diffusion of the carbides, ultimately hardening the material. A lower austenitizing temperature allows less diffusion of the carbides in comparison (lower hardness), but creates a material that is generally tougher and not as brittle [5]. The samples in this research were austenitized at 1500℉ for 30 minutes, allowing diffusion to occur faster. They were then quenched in oil to give a martensitic structure. Since this structure is known to be very brittle and cause cracking or shattering in the samples, the samples were quickly placed into their tempering furnaces.

Tempering is the last heat treatment step for the samples in this research. This was necessary in order to relieve the stresses in the samples caused by quenching. In order to achieve 600 H_v, the tempering temperature is 600ºF. For 400 H_v the tempering temperature is 1000ºF. Both samples were held at their respective temperatures for two hours. After tempering they were air cooled to room temperature.

In all, four electronic furnaces were used to heat treat the two samples. The furnaces were manufactured by CRESS; model number C410H/935. They operated on 230 AC volts and 10 amps. The room temperature in the laboratory was 67ºF and about 49 % humidity. Figures 12-15 below show the furnaces and oil bath.

Figure 12. Preheated furnaces for step 1 and 2.

Figure 13. Picture showing detail of furnaces.

Figure 14. Arrangement of furnaces and oil bath.

Figure 15. Detailed picture of setting and specs.

SURFACE PREPARATION

As explained earlier, surface preparation/surface roughness influences the measured hardness values. Table 6 shows that electrolytically polished samples at low loads were significantly and consistently lower than the mechanically polished samples

at low loads due to the electrolytically polished samples having a lower average surface roughness.

Table 6. Surface preparation effects on hardness [2].

	Average Hv		
	Mechanically Polished		Electro-polished
Metal	Stnd Loads	Low Loads	Low Loads
Lead	3.2	4.8 ± 0.42	4.4 ± 0.36
Tin	6.2	7.7 ± 0.15	7.3 ± 0.36
Copper	46	60 ± 4.3	44 ± 2.1
Mg3Al	53	60 ± 5.4	52 ± 5.1
Beta-Brass	175	175 ± 6.3	153 ± 11.2

Another source found that the variations in hyperbolic slopes of hardness indicate different degrees of work hardening that were caused by surface preparation. It was reported that the different stages of work hardening were reached by using various polishing methods [16]. A final source observed inconsistent results due to indents lying in the valley of the rough surface. This caused higher than expected hardness values because the cross-sectional contact area used in the calculation was less than the actual contact area [17].

In order to achieve reliable data in the nanoindentation test, the sample surface must be polished. This process requires experience, care, constant surveillance, and patience. Polishing usually involves holding the sample in contact with a polishing wheel supplied with a polishing compound. Each progression in polishing is accompanied by a smaller grit size. An important outcome considered when polishing was the modification of the surface properties due to strain hardening or cold-working. The greatest challenge in preparing the sample is to avoid significant deformation to its

surface. Excess deformation from polishing could lead to indentation size effects. One source claims that it is reasonable to assume that the polishing procedure affects the surface of the specimen to a depth of about the same size as the most recent nominal grit size used. It was concluded that for metal samples likely to strain-harden, the mechanical properties of the specimen over this depth range are expected to be influenced [10].

All of the samples used in this research underwent an elaborate surface polishing procedure. The steel samples were cut from a 1-inch diameter rod using a band saw. After the samples were rough cut, they were ground smooth. Figure 16 below shows the grinder used to complete this work.

Figure 16. Grinder used to smooth rough-cut samples.

The polishing began with the setup shown in Figure 17. The tantalum and O1 steel samples were first given a metallurgical mount in Bakelite. The three steel samples were then placed in the sample holder (six positions) opposite of each other, and the three other slots in the holder were occupied by blank Bakelite cylinders. The tantalum sample was polished with five other blank cylinders. The details of the polisher and holder are shown in Figure 17. The setup for the metallurgical mount is shown in Figure 18. The tantalum sample measured 12 mm in diameter and about 6 mm thick as received in the fully annealed state.

Figure 17. Autopolisher for sample preparation.

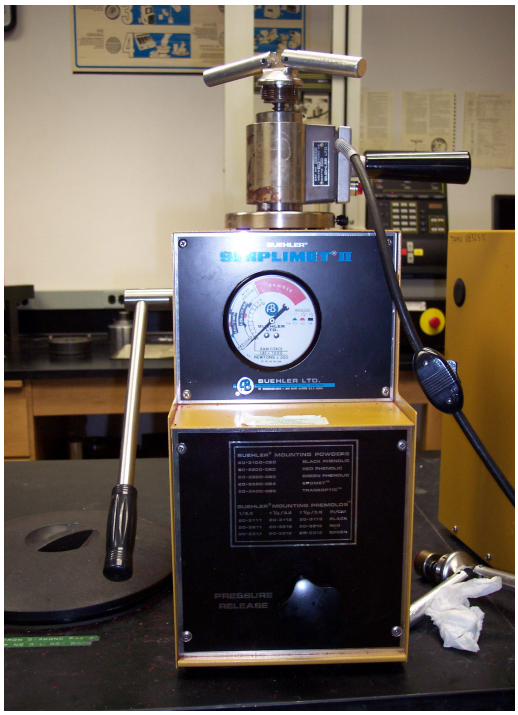

Figure 18. Metallurgical mount machine.

The first step in polishing was achieved with 600 grit silicon carbide metallurgical paper lubricated with mineral oil to prevent corrosion. The amount of

mineral oil depended on the force applied by the auto polisher, the speed of the rotary table, and the anticipated amount of time that the specimen would spend in the polisher. In this case the force was 8 pounds, the rotary speed was 30 RPM, and the time spent on the polisher was measured in 90-minute increments. If there was too much mineral oil, or the rotary speed was set too high, the polishing was largely ineffective. Once the surface of the samples appeared uniformly polished without any abnormal mars or scratches, the polishing proceeded to the next finer grit metallurgical paper. The 600-grit disc was followed by the 800, 1200, and 4000 grit silicon carbide metallurgical paper discs. The final polishing step utilized a fiber-polishing disc and a 0.050 μm alumina lubricating paste giving the samples a mirrored finish. The amount of time each sample required polishing was different depending on the hardness.

SURFACE ROUGHNESS

Surface roughness can cause uncertainty in contact area due to the asperity contact at very shallow indentation depths. At larger indentation depths the uncertainty in contact area is reduced. Since the roughness of the sample surface has a high potential to cause errors in the area function, surface roughness becomes a very important issue in nanoindentation. Surface roughness is characterized by the distribution of asperity height across the surface. There has been significant work done in this field since friction between surfaces is impacted by surface roughness [10].

A common expression for surface roughness is given below.

$$\alpha = \frac{\sigma_S R}{a_O^2} \tag{4.1}$$

Parameter α is the surface roughness, σ_S is the asperity height, R is the indenter radius and a_O is the contact radius obtained under the same load for a smooth surface. Here α depends indirectly on the indenter load. The equation also shows that the surface roughness increases with increasing indenter radius and decreasing indenter load. Therefore, for a given load, the Berkovich indenter will exhibit less severe effects from surface roughness than a spherical indenter. The intended effect of having a low surface roughness is to reduce the mean contact pressure by increasing the contact area, thereby reducing the penetration depth and cumulative modulus (E*) for a given load [10].

Figure 19 shows one of the smoothest surface finishes achieved using the before mentioned surface preparation technique (40 nm). All of the surface roughness measurements were taken using a Stylus Profilometer. The surface roughness goal was ≤ 100 nm roughness without causing significant surface deformation or cold work to the samples. Figure 20 shows the same measurement in greater detail.

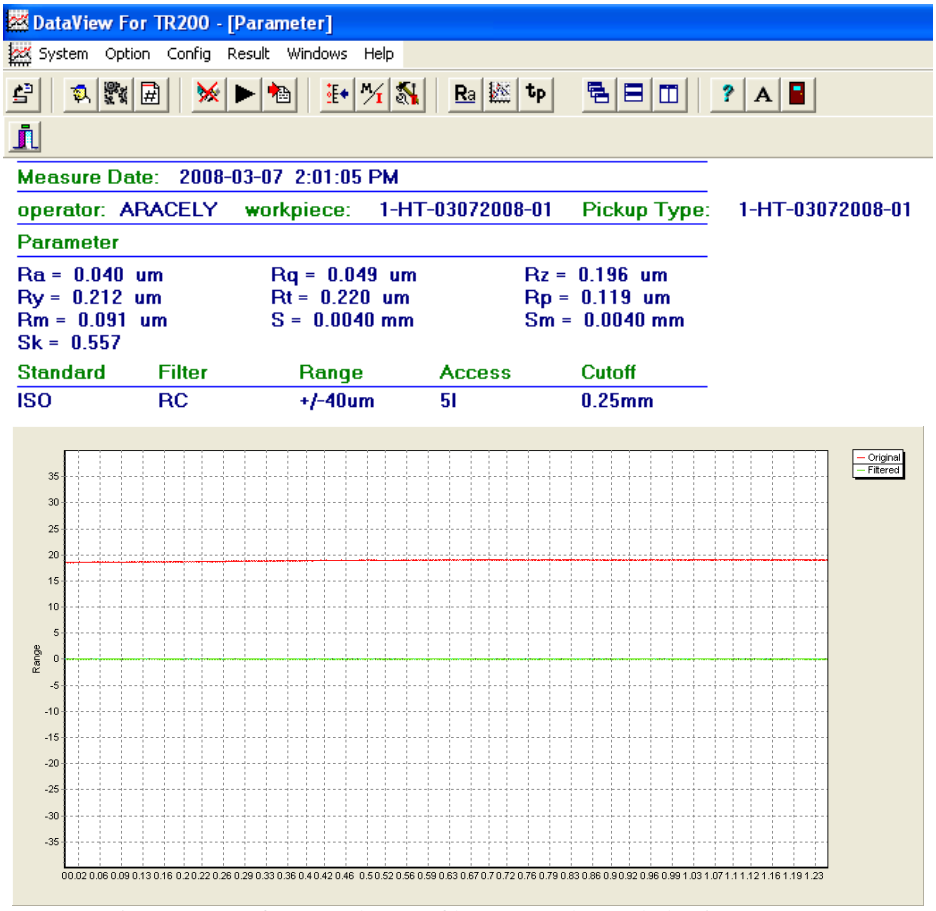

Figure 19. Surface roughness of heat treated sample having 400 Hv.

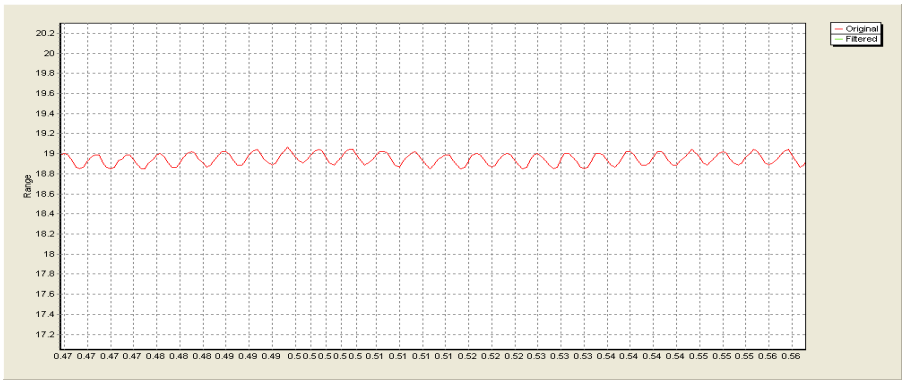

Figure 20. Detailed surface roughness graph of same of heat treated sample.

MICROSTRUCTURES

As mentioned earlier, the tantalum sample measured 12 mm in diameter and about 6 mm thick. It was received in the fully annealed state. The unalloyed, pure tantalum sample was cast into its final shape as opposed to powder metallurgy or electron beam melting. It is not shown in the figures below that the grain size in the sample has a very broad range. However, it is shown in Figure 21 and Figure 22 that a second phase exists on the sample. The darker shaded areas depict oxide particles on the surface.

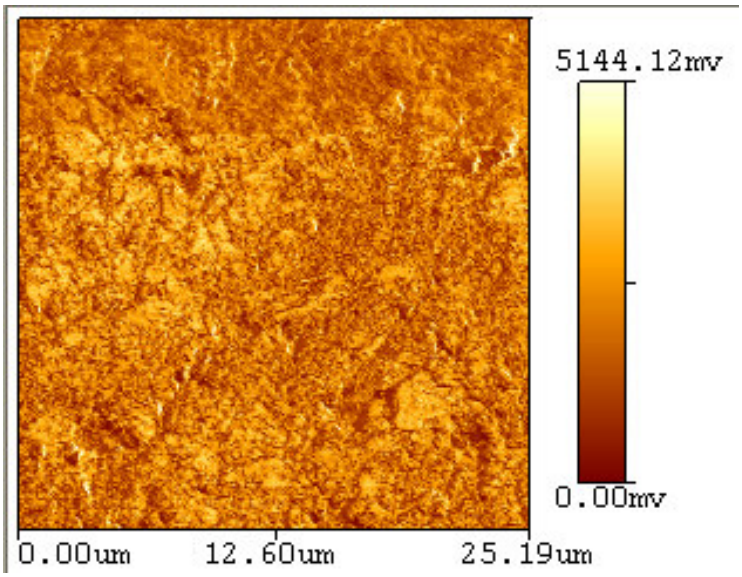

Figure 21. 25 μm AFM image of phases on the tantalum sample.

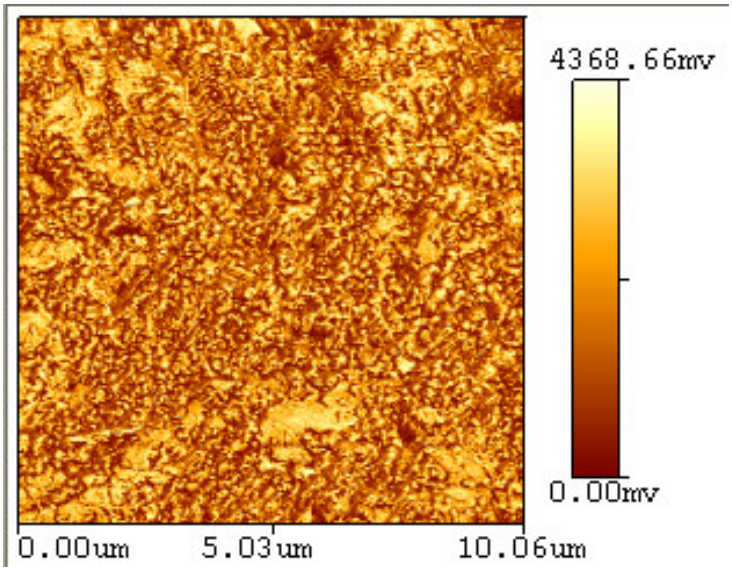

Figure 22. 10 µm AFM image of phases on the tantalum sample.

Three oil-quenched O1 tool steel samples were used in the research, two samples in this research were heat treated and one was not. The non-heat treated sample was left in the condition that all of the steel samples were received, which was the fully annealed state. In this state (as purchased) the steel is easier to machine. However, the other two samples were heat treated yielding a different microstructure. One of the samples was austenitized at 1500°F for 30 minutes, oil-quenched, and tempered at 600°F for 2 hours. This microstructure appeared to have spheroidal carbide particles in a tempered martensite matrix. The other sample was austenitized at 1500°F for 30 minutes, oil-quenched, and tempered at 1000°F for 2 hours. This microstructure also appeared to have spheroidal carbide particles in a tempered martensite matrix. Figure 23 shows such microstructural features as an example. The microscopic image shows the sample at 1000 times magnification. The O1 steel sample in the figure was austenitized at 1500°F,

oil-quenched, and tempered at 425 °F. This structure has large spheroidal carbide particles in a matrix of tempered martensite.

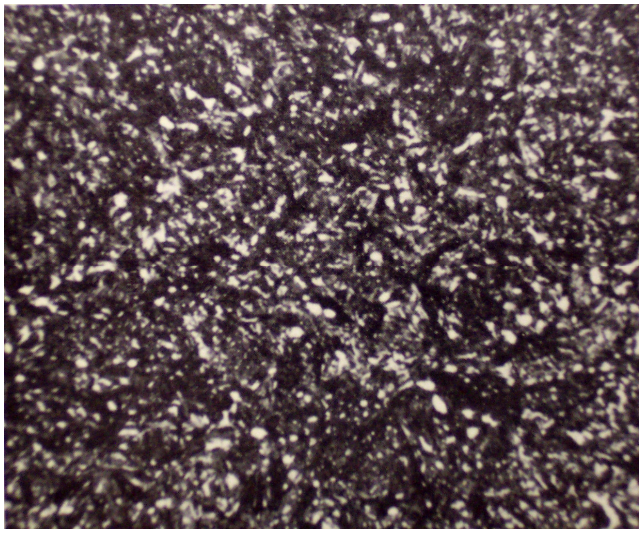

Figure 23. Structure of heat treated O1 steel at 1000x [18].

AFM images were taken of the O1 tool steel samples using both close contact and non-contact modes. Figure 24 is an image of the surface of one of the samples using the non-contact mode. This image serves to show the topography of the sample surface, not necessarily different phases. Some of the features in the image show polishing patterns, other features show martensite needles, and the smooth looking areas aggregate the tempered martensite steel matrix. The arrows in the figure point out a couple of the distinguished martensite phases that are within three μm across.

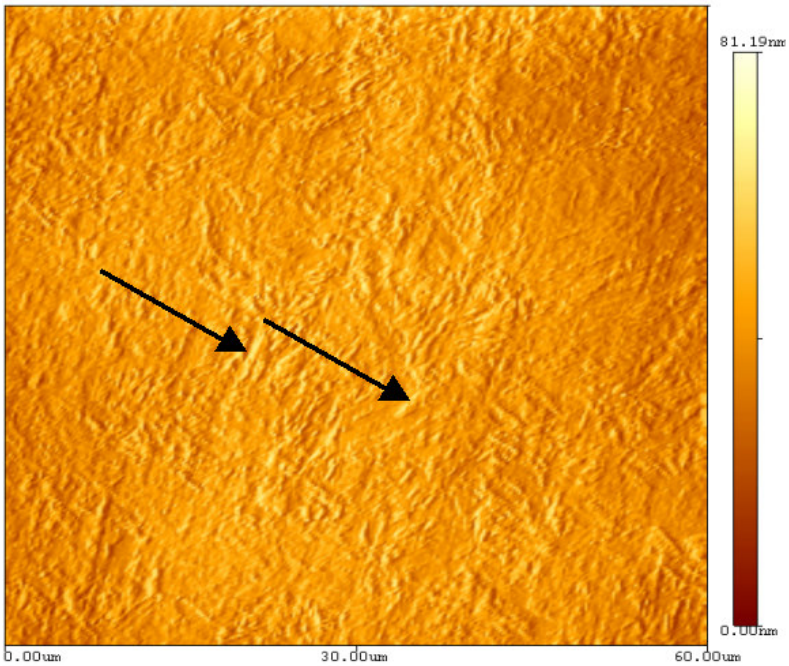

Figure 24. Non-contact mode AFM image of O1 tool steel sample at 60 µm.

Figure 25 is an image of the same surface of the sample used in Figure 24 using the non-contact mode. However, this image shows the topography of the sample surface at a sixth of the scale. Polishing patterns and shallow scratches are easily seen in the image. The lighter and darker features are different surfaces of the tempered martensite steel matrix. Spheroidal carbides cannot be easily distinguished from this image. Consistent with Figure 24, some of the distinguished martensite phases are between three and five µm across.

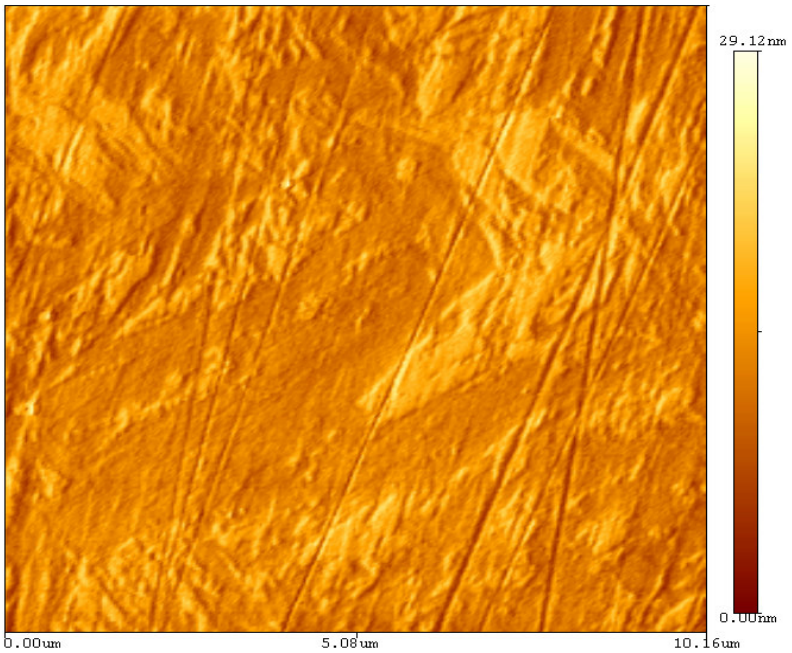

Figure 25. Non-contact mode AFM image of O1 tool steel sample at 10 µm.

Figure 26 is an image of an O1 tool steel sample using the close contact mode AFM. This image shows the phases and topography of the sample surface at a very fine scale. Polishing patterns and shallow scratches are not easily seen in this image. What can be recognized in this image are the tempered martensite phases and spheroidal carbides. The lighter shaded sharp and linear features represent the martensitic phases, and the white dots represent the spheroidal carbides. According to the scale, the size of these carbides may be about 500 nm in diameter. The difference in the level of detail and sharpness between Figures 25 and 26 are a function of both scanning speed and test mode.

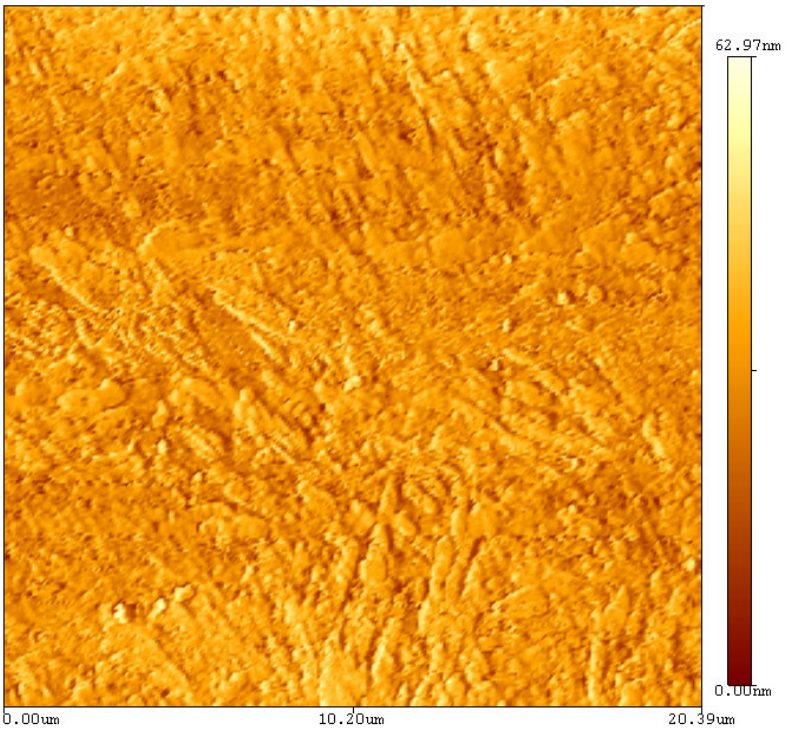

Figure 26. Close contact mode AFM image of O1 tool steel sample.

The AFM instrument used in this research is shown below with one of the O1 tool steel samples mounted in red Bakelite (Figure 27). The manufacturer of the instrument is Pacific Nanotechnology. Two modes were used. The morphological image shows the surface roughness using close contact mode. The phase image distinguishes different microstructures through the material's response of the probe tapping on the surface. The close contact mode AFM probe will be used for this type of analysis. The average surface roughness for the surface areas shown in Figures 30-32 ranges from 2.5 nm – 6 nm. The smoother measurements were taken from the smaller scanned images.

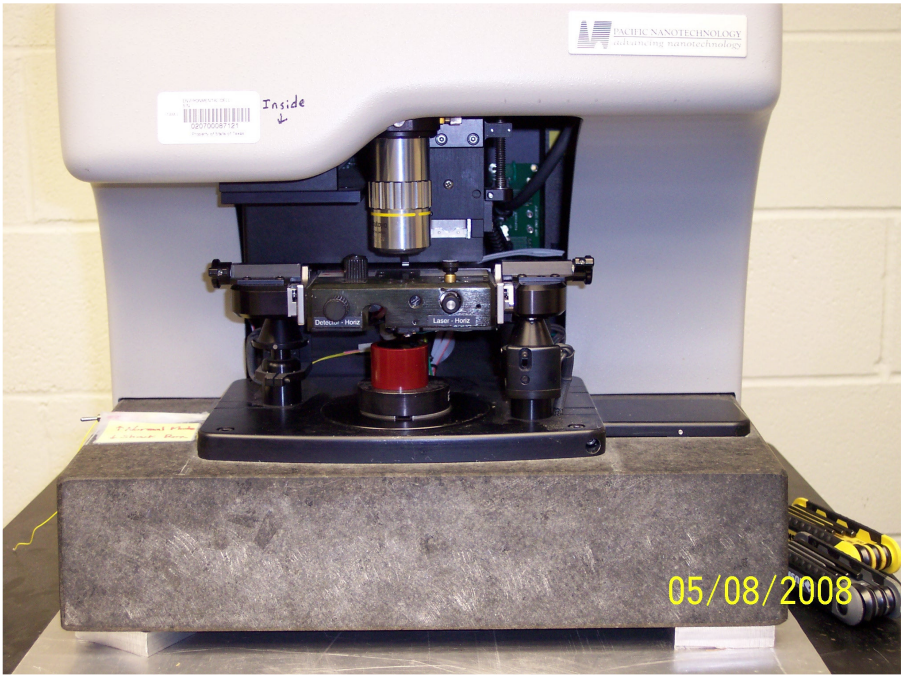

Figure 27. Photo of the AFM instrument and O1 tool steel test sample.

CHAPTER V

RESULTS

The data acquired from both testing techniques were analyzed. The first data collected was the nanoindentation data. The data files for this test are very large, the first step in analyzing the data was to organize all of the raw data measurements taken by the instrument and locate the critical parameters that the instrument used to calculate the hardness values. Once these parameters were found, the tip rounding and pile-up dimensions (which the instrument does not account for) were added to the penetration depths used to calculate the area using equation (7.7). Once this was known the true hardness values could be calculated using equation (7.8).

The procedure mentioned above yielded nine hardness values for each sample at each load setting. These values are found in Figures 28, 30, and 32. The task at this point was to take all 45 hardness values for each sample and determine the sample's true average hardness. This was determined by first generating the hardness versus penetration depth graphs shown later in this chapter. The data points of each dataset that suggested a lower limiting hardness value were then chosen to be used in the average hardness calculation. If all or several of the individual load datasets appeared to be at the lower hardness trend, then the hardness values from those datasets were averaged. This technique was chosen due to the asymptotic (leveling) trend in the data that was formed by ISE. The lower limiting values minimized ISE in the average hardness over the loads tested, giving a more accurate hardness measurement. All data sets showed this minimizing effect at greater depths (greater loads). This technique yielded one true

average hardness value for each sample for the loads tested. These values are listed in Table 7 below. The data acquired from the Rockwell tester was straightforward and required no manipulation beyond the standard conversion to Vickers hardness scale.

Table 7. Nanoindentation hardness test data for the O1 tool steel samples.

O1 Tool Steel Nanoindentation Data					
HT 2		HT 1		N-HT 1	
HIT	kg/mm^2	HIT	kg/mm^2	HIT	kg/mm^2
964	858 ± 84	838	732 ± 41	360	314 ± 15

All three O1 tool steel samples were tested at maximum loads progressing from 5000 μN to 9000 μN in 1000 μN increments. Although the tests were performed using the same machine, the 5000 μN datasets were acquired March 19, 2008 and the 6000 μN - 9000 μN datasets were acquired April 2, 2008. Each indent had a 10 second loading duration and a 10 second unloading duration. Therefore, for the 5000 μN maximum load setting, the loading rate was 500 μN/sec. For the 6000 μN maximum load setting, the loading rate was 600 μN/sec, and so on. There were no hold points for any of the indents taken. For all tests, the temperature of the room, equipment, and samples were stabilized at 74ºF with a humidity of 47%. For each sample, a 3-by-3 matrix was used for measuring the hardness at each load setting, giving nine indentations per load setting, per sample. This results in 45 indentations per O1 sample and 135 total indentations for all O1 samples.

Figure 28 shows nanoindentation test data for the non-heat treated O1 sample 1. As a result of the hardness values increasing with decreasing displacement, there is an

apparent ISE at each load dataset and over all datasets. However, there did not appear to be any oxide effects in the data. One reason for this is due to the sample being polished a few hours before being tested, thereby minimizing oxide formation. If oxides were present, they would not be evident in the graphs shown here since the thickness of surface oxides were penetrated within the first 20 nm of an indention. The average nanoindentation hardness for non-heat treated O1 sample 1 is $314\,kg/mm^2$. Figure 29 shows a set of load-displacement curves for the non-heat treated O1 sample 1. The curves of the loading and unloading cycle appear to be uniform and smooth for the most part, indicating that there were not any materials related errors associated with the test. For the given maximum test force the maximum displacement appears to range from 289 nm to 297 nm.

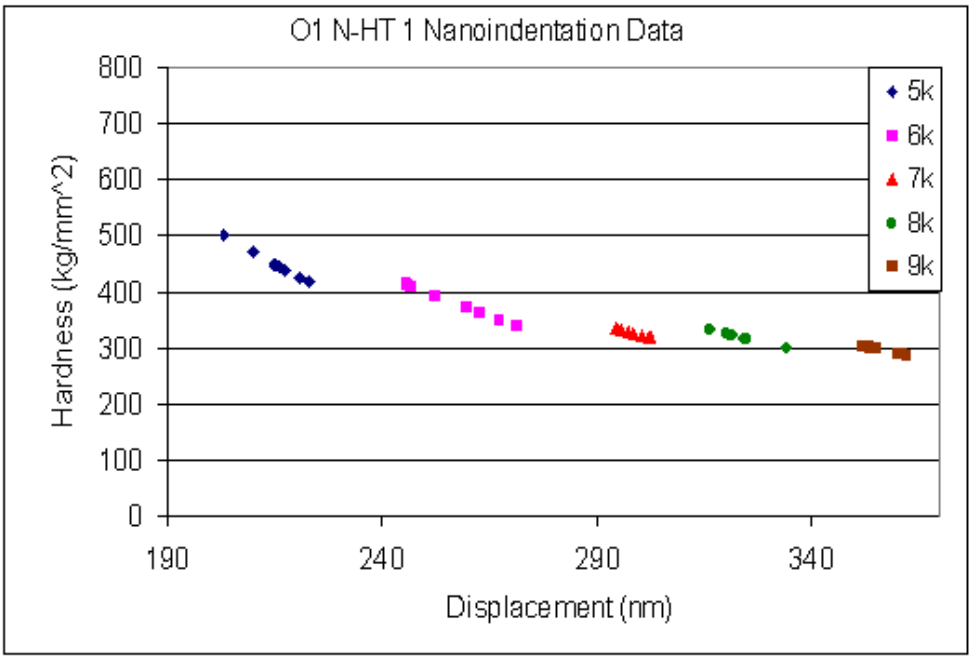

Figure 28. Nanoindentation test data for the non-heat treated O1 sample 1.

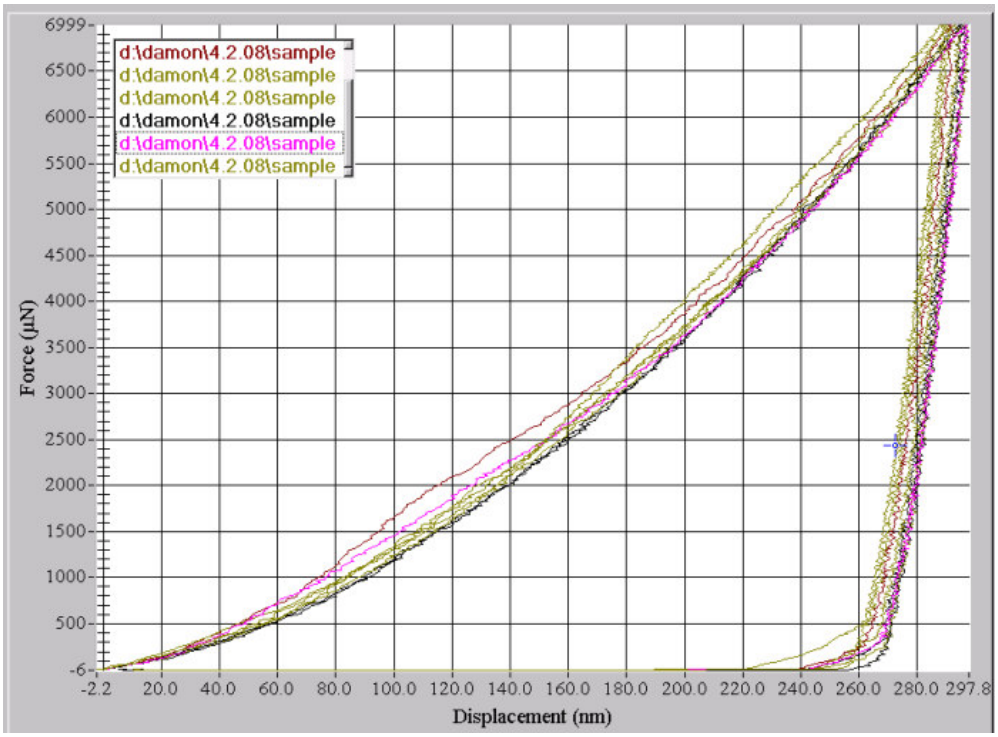

Figure 29. Non-heat treated O1 sample 1 load-displacement curves at 7k µN force.

Figure 30 shows nanoindentation test data for the heat treated O1 sample 1. There is an apparent ISE at each load dataset, but there did not appear to be any oxide effects in the data. This is due to the minimal time between polishing and testing the sample. The average hardness measurements do not appear to be broad over the range of test loads. This places confidence in the data for measuring the true hardness of the material. The average nanoindentation hardness for heat treated sample 1 is $732\,kg/mm^2$. Figure 31 shows a set of load-displacement curves for the heat treated O1 sample 1. The curves of the loading and unloading cycle appear to be very smooth and uniform, therefore causing no alarm in the quality of the data acquired. For the given

maximum test force the maximum displacement appears to range from 173 nm to 182 nm.

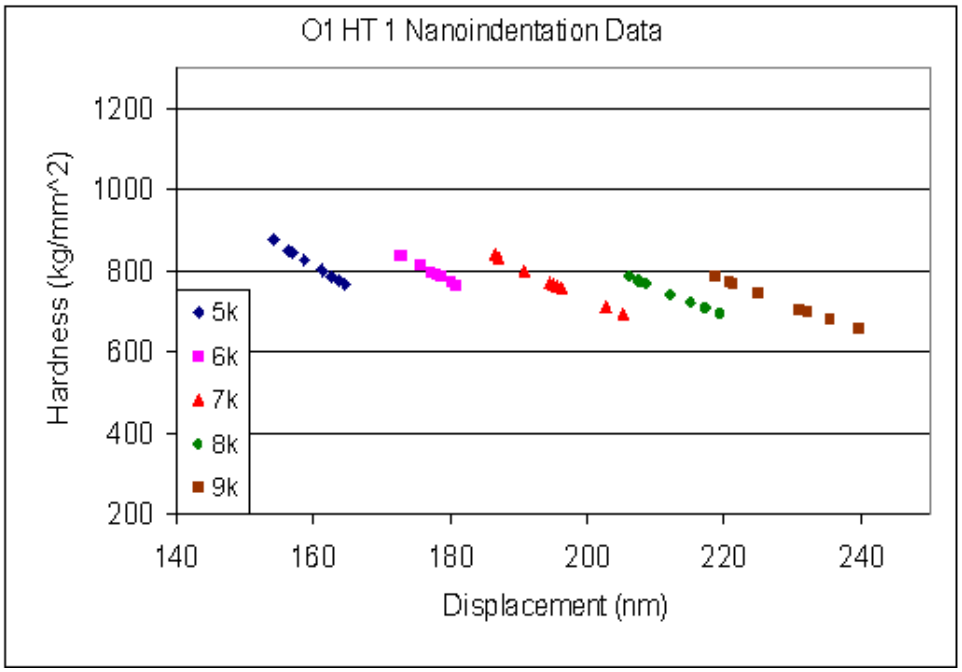

Figure 30. Nanoindentation test data for the heat treated O1 sample 1.

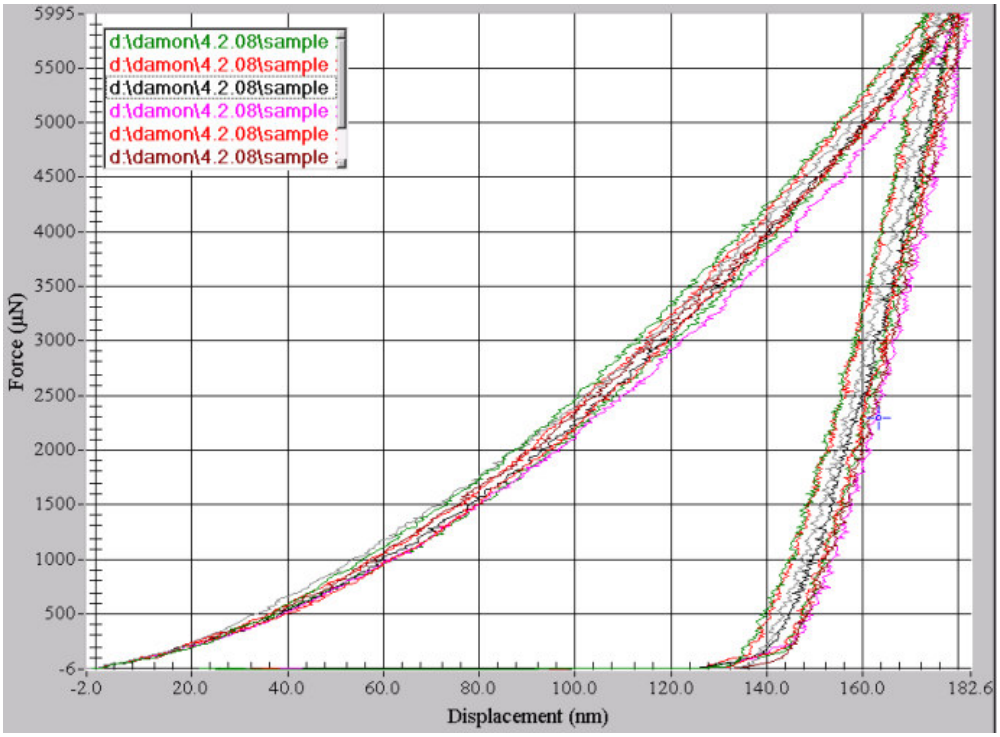

Figure 31. Heat treated O1 sample 1 load-displacement curves at 6k µN force.

Figure 32 shows nanoindentation test data for the heat treated O1 sample 2. There is an apparent ISE at each load dataset, but there did not appear to be any oxide effects in the data. The reason for this is similar to that for the other samples, very small amount of time between polishing and testing. The 9000 µN dataset shows a broad range of hardness and displacement measurements relative to the other datasets. The most likely cause for this material response is the indenter penetrating different microstructures. Possible microstructures for high hardness and low penetration depth responses include a high density of spherical carbide in the vicinity of the indent, and indents taken in the tempered martensite matrix. Microstructural features contributing to low hardness and higher penetration depths include indents taken in dislocations and

grain boundaries. The average nanoindentation hardness for O1 heat treated sample 2 is 858 kg/mm^2 . Figure 33 shows a set of load-displacement curves for the heat treated O1 sample 2. The curves of the loading and unloading cycle appear to be very smooth and uniform, therefore causing no alarm in the quality of the data acquired. For the given maximum test force the maximum displacement appears to range from 186 nm to 194 nm.

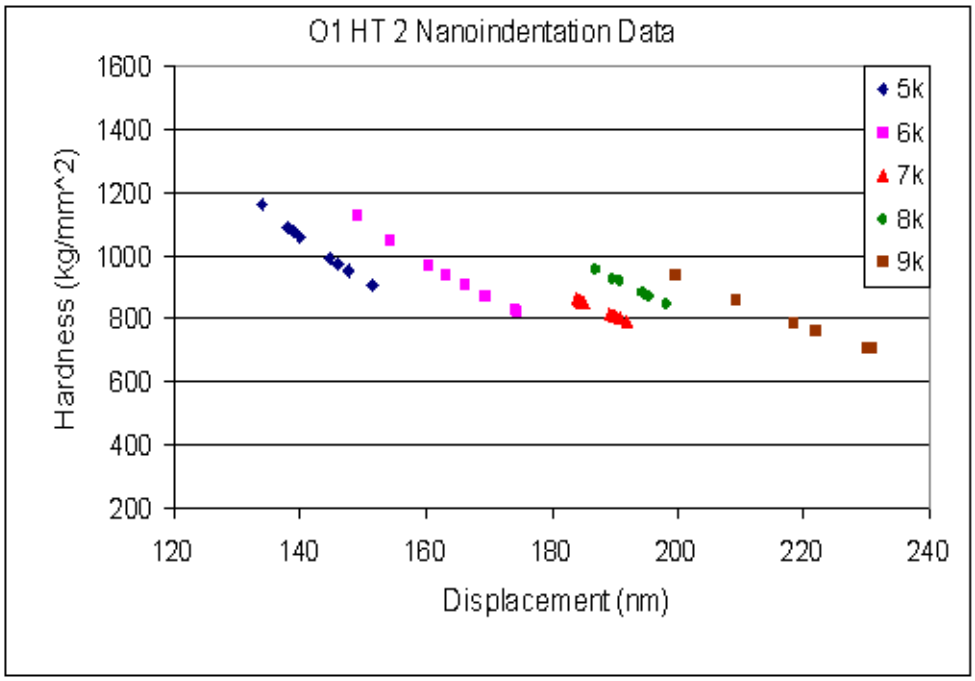

Figure 32. Nanoindentation test data for the heat treated O1 sample 2.

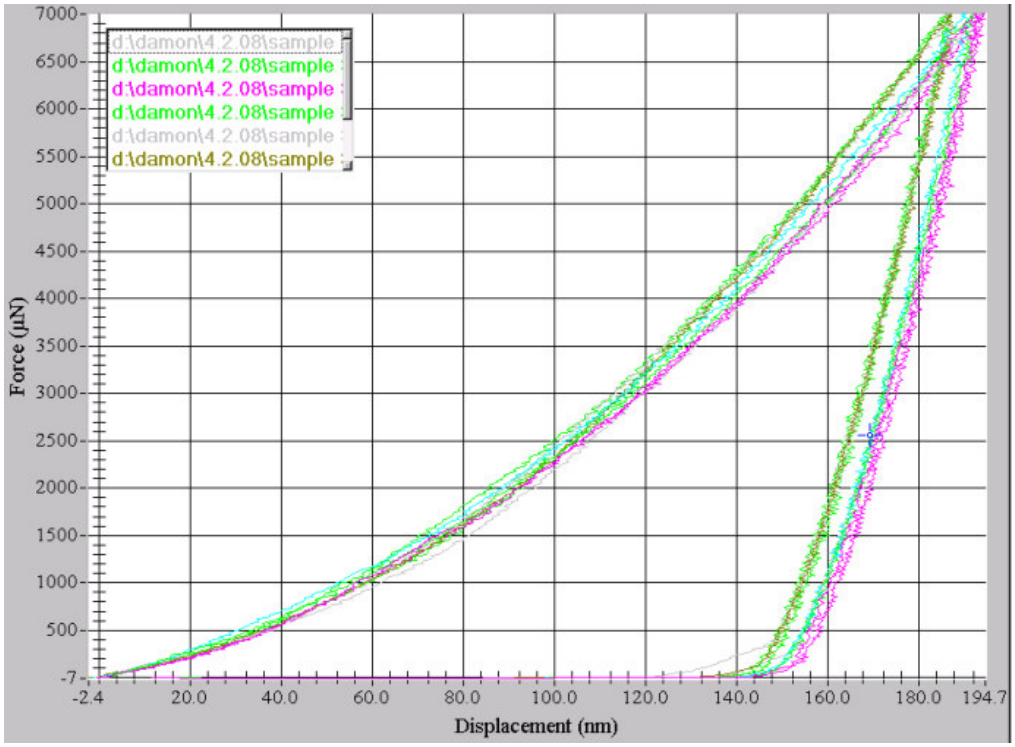

Figure 33. Heat treated O1 sample 2 load-displacement curves at 7k µN force.

Figure 34 shows nanoindentation test data for the tantalum sample. The set of data points at each load setting represents data taken for one indent (five indents total) as opposed to the steel samples where one data point corresponded to one indent. There is a slight ISE over all of the test loads, however, there did not appear to be any oxide effects in the data. This is due to both minimal oxide initiation and growth time before testing, and the noble, low oxide forming nature of the material. The average nanoindentation hardness for the tantalum sample is $240\,kg/mm^2$.

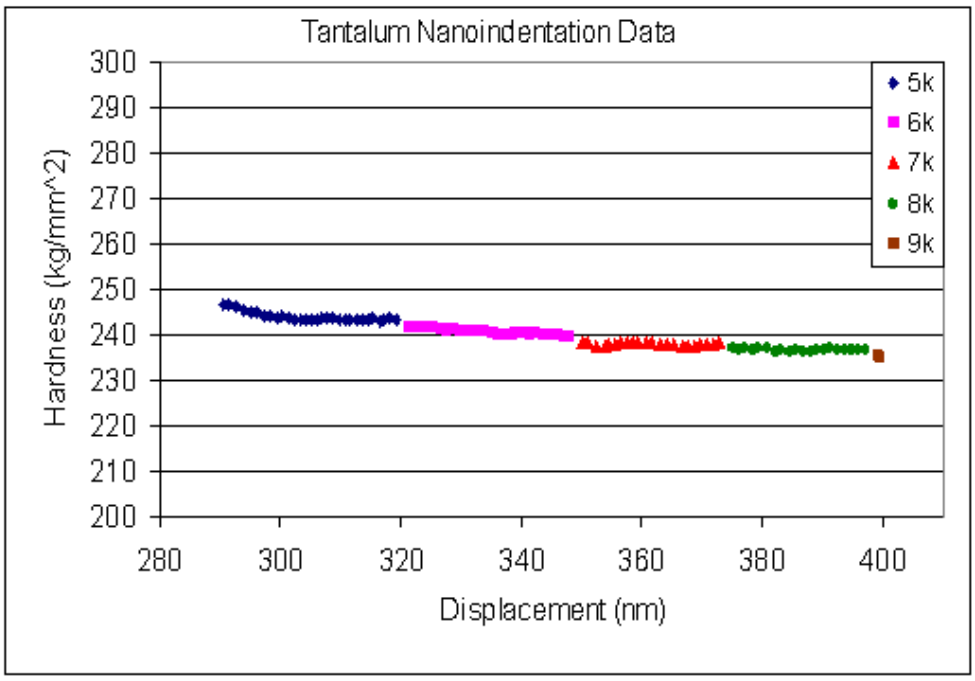

Figure 34. Nanoindentation test data for the tantalum sample.

All O1 samples were tested immediately after being polished. The 9000 μN dataset for non-heat treated O1 sample 1 was the last to be acquired in the O1 sample test series. This dataset was acquired within 14 hours of being polished. This test condition accounts for not having apparent oxide effects in the data. Table 7 shown on page 58 shows the true average hardness values determined by the nanoindenter, and then the corrected true average hardness values in kg/mm^2 (Vickers hardness units).

The macroindentation testing was completed for all samples using the superficial Rockwell N scale. The load cycle begins with a 3 kg minor load and then a 15 kg maximum load. For each sample, 3 indentations were made and recorded. The room temperature in the laboratory was 67 ºF and about 49% humidity. Figure 35 shows macroindentation test data for the O1 samples acquired on April 21, 2008, and the

tantalum sample data acquired on May 8, 2008. The hardness ranges of the steel samples appear to be 200-650 H_v, which was roughly the heat treatment goal for the research. After each test, the superficial Rockwell value was converted to the Vickers scale according to ASTM E 140 standards. All samples were tested immediately after being lightly re-polished.

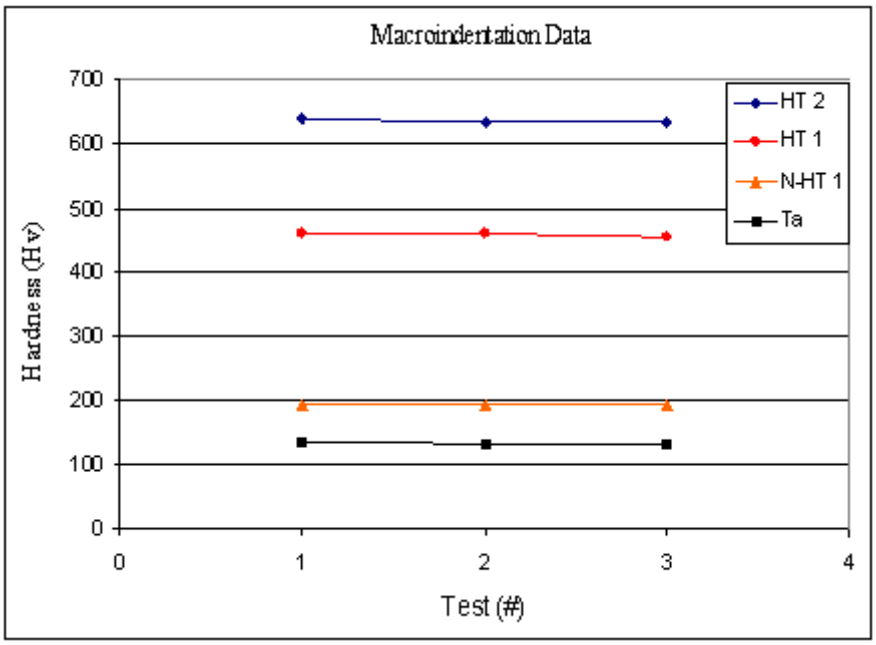

Figure 35. Macroindentation hardness test data for all samples.

Table 8 below shows the macroindentation hardness values for the tool steel samples in both scales and the average hardness for each sample. Non-heat treated sample 1 Vickers hardness values were calculated using the Rockwell 15N-to-Vickers conversion equation (shown below in equation 5.1) according to the ASTM E 140 standard. Table 9 shows the hardness values for the tantalum sample in both scales and

the average hardness for the sample. These hardness values were also calculated using the Rockwell 15N-to-Vickers conversion equation according to the ASTM E 140 standard. This equation has a R^2 value equal to 0.9998, thereby giving great confidence in accurately characterizing a hardness value or a small range of values [*19*].

$$Hv^{-1} = 2.59838\,x10^{-2} - (4.31497\,x10^{-4}(HR15N)) + (1.75469\,x10^{-6}(HR15N)^2) \quad (5.1)$$

$$R^2 = 0.9998$$

Table 8. Macroindentation hardness test data for the O1 tool steel samples.

O1 Tool Steel Macroindentation Data						
	HT 2		HT 1		N-HT 1	
	HR 15N	Hv	HR 15N	Hv	HR 15N	Hv
1	89	638	83.6	461	65.7	192
2	88.9	633	83.6	461	65.6	191
3	88.9	633	83.4	456	65.6	191
Avg.	88.9	635	83.5	459	65.6	191

Table 9. Macroindentation hardness test data for tantalum.

Ta Macroindentation Data		
	HR 15N	Hv
1	55.3	134
2	55.2	133
3	55.2	133
Avg.	55.2	133

CHAPTER VI

FACTORS AFFECTING NANOINDENTATION HARDNESS

During testing there are many factors affecting the resulting hardness number. Nonmaterial property related errors include equipment calibrations, vibration during testing (including indentation time), and indenter shape. The most impactful errors of this type are incorrect depth measurements. Material property related errors in the sample include surface preparation methods, orientation properties of the material, material hardness heterogeneities, elastic recovery, and nearby plastic deformation from indentation testing or handling. The most impactful material related errors are indentation size effects (ISE) and the phenomena explained below, piling-up and sinking-in. These errors are the subject of continued research, the ultimate goal of which is to accurately account for them. A final error that can be introduced into the measurements is thermal expansion or contraction. This is termed thermal drift and it may be avoided by allowing the sample and the instrument to achieve thermal equilibrium [20].

THERMAL DRIFT

To explain thermal drift a little more thoroughly, there are two commonly known types of thermal drift behavior that may occur in nanoindentation testing. One type is creep within the sample caused by plastic flow. Although not tested in this research, creep can be observed when a load is held constant on the indenter and the depth readings increase as the indenter sinks into the specimen. Another type of drift is a

change in the dimensions of the instrument due to thermal expansion or contraction of the apparatus. This behavior causes an observed change in depth under a constant load and is undistinguishable from creep. These depth changes cause a thermal drift error on the actual penetration depth. This type of drift can work both ways though. The other way is from the generation of heat within the plastic zone of the indentation. One source claims that the temperature rise within the specimen material is quite substantial, approximately 100℃. The author added that the volumes of material are so small however, that any change in linear dimension of the specimen would be less then 0.1% of the overall penetration depth. Although this effect is minuscule, the author explains that localized high temperatures within the specimen may affect the viscosity and hardness of the material [10].

Penetration depth data can be adjusted if the drift rates are determined. This is achieved if at some point during the test the operator can capture the depth data over time when the load is constant. The required data can be captured at maximum load or at the end of unloading from maximum load. For calculation, it is recommended to use the data at the final unload increment. This is because creep within the material is less likely to occur at low loads [10].

COMPLIANCE FACTOR

The compliance of the instrument is defined as the deflection in the loading frame, indenter shaft, and sample mount. The applied test force affects the sample surface and parts of the testing machine, which are all elastically deformed. This elastic

deformation causes an increase in the measured indentation depth that is not experienced at the indentation contact. The compliance of the loading frame is quantified as the deflection of the instrument divided by the load. The sample and the loading frame contribute to the measured unloading stiffness during the indentation test. Analytically, the specimen, indenter, and load frame are considered to be springs in series. That is, the compliance of each is added to give the total compliance measured by the instrument. The test samples are held firmly to minimize compliance in the sample mount. Prior to testing, the samples are mounted on the stage using superglue [10]. Figure 36 shows the meaning behind deflection of the loading frame.

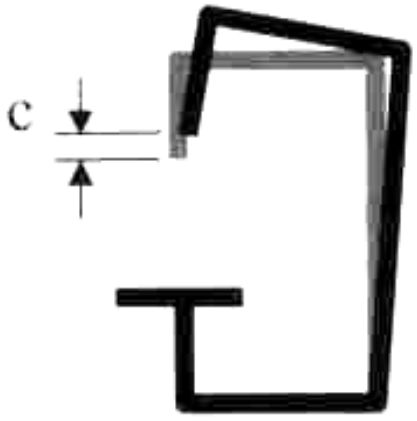

Figure 36. Effect of load frame deflection [10].

GEOMETRIC CORRECTION FACTOR

As explained earlier, in nanoindentation tests the contact area is found using the penetration depth and the indenter geometry data. The areas given in Table 10 assume that the geometry of the indenter is geometrically flawless, which is understandably

rarely the case. A main contributor to this reality is the crystal anisotropy of the diamond indenter. To account for this, the correction factors listed in Table 10 must be used. The correction factor is the ratio of A/Ai. The actual area of contact is A, and the ideal area of contact is Ai.

Table 10. The projected areas of contact for some common indenters [10].

Indenter type	Projected area	Semi-angle θ (deg)	Effective cone angle α (deg)	Intercept factor* ε	Geometry correction factor β
Sphere	$A \approx \pi 2Rh_p$	N/A	N/A	0.75	1
Berkovich	$A = 3\sqrt{3}h_p^2 \tan^2\theta$	65.27°	70.3°	0.75	1.034
Vickers	$A = 4h_p^2 \tan^2\theta$	68°	70.3°	0.75	1.012
Knoop	$A = 2h_p^2 \tan\theta_1 \tan\theta_2$	$\theta_1 = 86.25°$, $\theta_2 = 65°$	77.64°	0.75	1.012
Cube Corner	$A = 3\sqrt{3}h_p^2 \tan^2\theta$	35.26°	42.28°	0.75	1.034
Cone	$A = \pi h_p^2 \tan^2\alpha$	α	α	0.727	1

Figure 37 shows that for the same penetration depth, the actual area of contact is larger than the nominal dimensions of the indenter.

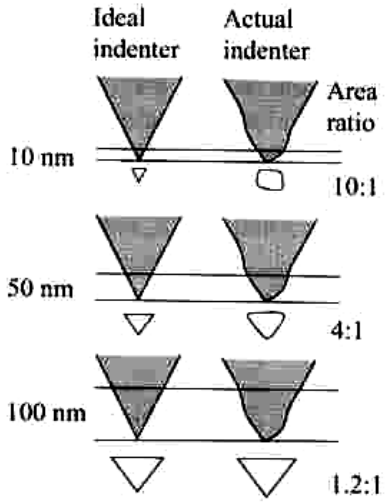

Figure 37. Comparison of contact areas between an ideal and real conical indenter [10].

The actual area can be measured directly using AFM or SEM, which can then be used to determine the correction. However, in this research the correction factor is found by performing a series of indentions with various maximum loads on standard blocks. If A/Ai is greater than one, the actual indenter has a larger tip radius than its nominal value. Large A/Ai values at low penetration depths are a sign of bluntness in the indenter tip [10].

TIP ROUNDING

The Berkovich indenter used in this research and all indenters in general will experience tip rounding at some point. The tip radius for a Berkovich indenter is usually in the range of 50 to 100 nm for new indenters, and 200 to 300 nm for used indenters. Figure 38 illustrates the error that is associated with tip rounding.

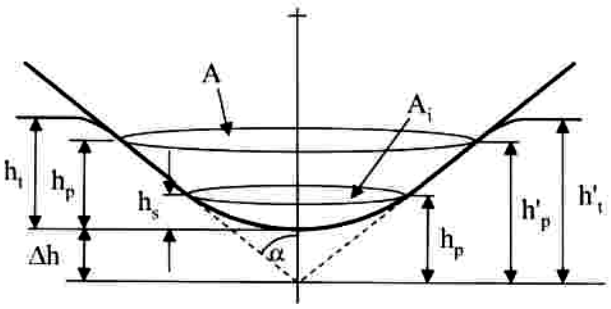

Figure 38. Indentation using a conical indenter [10].

In the figure above, let Δh represent the error in the tip displacement measurement. As a result, the total and residual indention displacements are in error by that amount. However, the significance of the error becomes smaller as the total penetration depth becomes larger. More specifically, as the total penetration depth becomes larger, the Δh impact becomes smaller, and the area function A/Ai approaches unity [10]. In this research the effects of tip rounding are accounted for in the hardness calculations and not by the instrument.

PILING-UP AND SINKING-IN

The phenomena of piling-up and sinking-in were briefly introduced earlier. Now they will be discussed in further detail. When an indentation into a material involves plastic deformation the material may either sink in or pile up around the indenter. The extent of pile-up or sink-in was found to depend on the E/Y ratio and level of strain hardening of the sample material [10]. Another reliable prediction of this phenomenon comes from the relationship of the residual penetration depth (h_r) and the total penetration depth (h_t). That is, piling-up is expected when $h_r/h_t > 0.7$ and sinking-in

where $h_r/h_t < 0.7$. It was also found that pile-up around the indenter caused the actual contact area to be larger than the calculated cross-sectional contact area. This value led to a higher than anticipated nanoindentation hardness [21].

For metals with low E/Y values, sinking-in occurs due to the elastic deformation of the indention being spread from the indenter. These annealed metals exhibit strain hardening, where the yield strength increases with strain increases. That is, the metal within the plastic zone of an indention becomes harder as the amount of deformation increases. Moreover, the outermost material of the plastic zone is then softer and more susceptible to plastic deformation with progressive indentation. Since the material farther away from the indentation is softer, the material near the indenter is forced to sink-in [10].

In comparison, piling-up is most evident for strain hardened (non-strain hardening) materials with a high E/Y ratio. Strain hardened metals are expected to experience piling-up because plastic deformation develops near the indenter. Sinking-in is more evident for non-strain hardened (strain hardening) materials with a low value of E/Y. The surface of the sample is typically drawn inwards and downwards underneath the indenter. These effects are illustrated in Figure 39 [10].

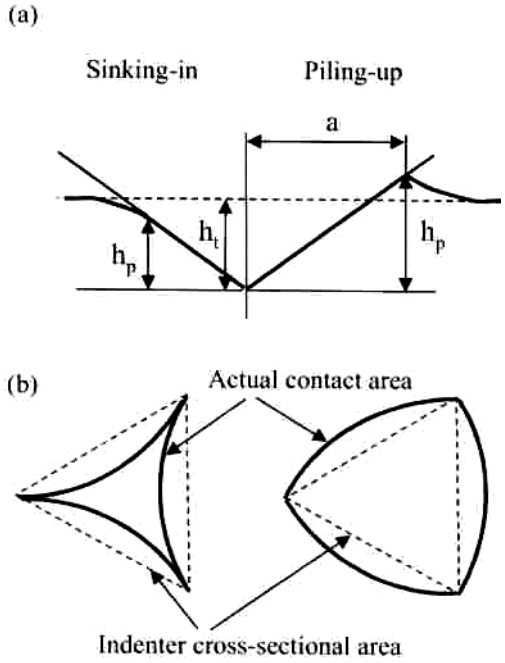

Figure 39. (a) Cross-section of an indentation (b) Piling-up and sinking-in effects on the contact area for the same penetration depth [10].

Other material factors influencing hardness measurements that were not explained above will be mentioned now. One factor affecting the variation in material behavior and hardness are material heterogeneities in the sample. These variations can occur from heat treatments or cold work, which affect the elastic and plastic properties of the metal. The crystallographic orientations for anisotropic metals may also cause heterogeneities. Therefore, hardness may be a function of grain orientation in the presence of an indentation. A final factor listed here may be one that is caused by performing indentation tests too closely. The already plastically deformed material will generate false hardness measurements if the indentations are taken in close proximity to one another [10].

INDENTATION SIZE EFFECTS

The tantalum sample used in this research is known to be a homogeneous, isotropic material. Therefore, the expectation is that only one value for hardness will be found for any given penetration depth. According to another phenomena, indention size effect (ISE), this expectation may be too simplified. The indentation size effect occurs when an increase in indentation hardness is observed when reducing the penetration depth [22]. Several mechanisms to explain this behavior have been proposed. It was initially believed to be inadequate measurement capabilities [23], and then another proposal suggested the presence of oxides or chemical surface contaminants [24]. The next suggestion was friction created between the specimen and the indenter [25], followed by another suggestion that the increased dominance of edge effects was responsible for ISE [26]. However, a large number of studies (including this one) propose a strain gradient theory to explain the effect [14,27-30].

For highly active materials in the atmosphere, the reason for the measurement anomalies in material behavior arises from the presence of an outer thin oxide layer. This layer has significantly different mechanical properties than pure tantalum, for example. However, the most common indentation size effect is the error in the area function of the indenter, particularly at very small values of penetration depth. In materials that exhibit ISE, plastic flow may depend on the magnitude of a strain gradient that may be present in the material. These gradients are said to appear at the crack tip where the dominant stress states are changing. ISE are reported to be more noticeable in materials with lower hardness [10]. One source reported that there is a critical indentation depth, below which

the surface effects dominate the response. The surface effects include energy loss from friction stresses, plastic deformation, and surface tension. Bulk effects were said to dominate at greater depths [10,31].

CHAPTER VII

INDENTATION CONTACT ANALYSIS

STRESS ANALYSIS OF INDENTATION CONTACT

The three-sided Berkovich indenter and the four-sided Vickers indenter are the most common types of pyramidal indenters. They are shown in Figures 40 and 41 below.

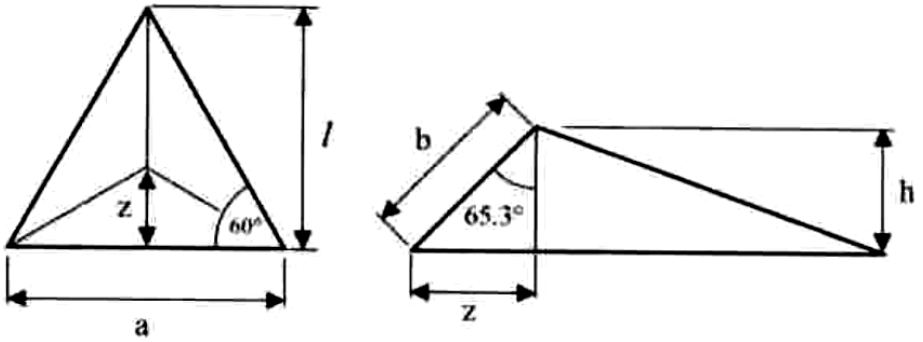

Figure 40. Three sided Berkovich indenter [10].

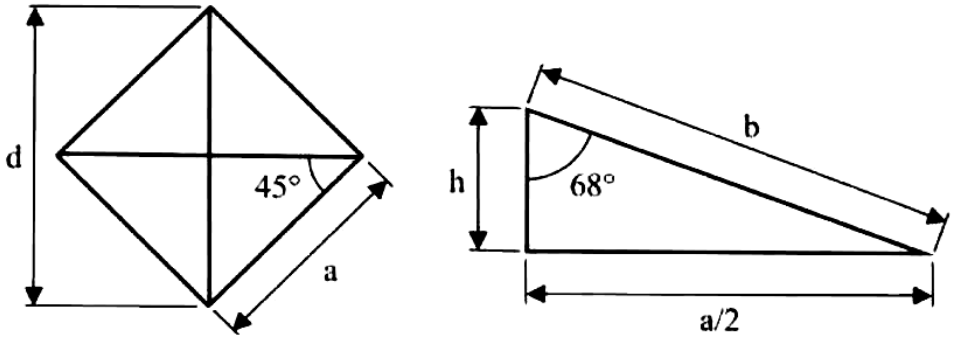

Figure 41. Four sided Vickers indenter [10].

The main focus in the test is the contact area determined from the indenter geometry, also known as contact mechanics. In order to quantify the contact of a non-axial symmetric indenter (pyramidal indenter), the indenter must be thought of as having an

axial symmetric geometry. Therefore, indentation testing using a pyramidal indenter becomes treated as indentation testing using a conical indenter. The feature that allows such a solution is the effective cone angle, which provides the same area-to-depth ratio between the two indenters. That is, the ratio of pyramidal diagonal length and conical indenter contact radius to the depth of the indentation are constant for increasing load. The conversion to an equivalent axial symmetric geometry has found wide acceptance [10]. Table 10 on page 71 lists the projected areas of contact for some common indenters.

One study investigated the standard deviations in the nano and microindentation hardness measurement methods. The study focused on the significance of the geometrical deviations in the nanoindenter affected by the indentation. In depth ranges less than 200 nm, it was found that the geometrical deviations of the indenter have a greater influence on the measured hardness values than the uncertainties that can be attributed to the nanoindenter instrument [32]. In summary, for microindentation hardnesses, the relative hardness uncertainty as a function of indentation depth was found to be less than 8%. Uncertainty in the area function of nanoindentation hardness was found to range from 8% to 18% depending on the penetration depth [32]. As seen in Figure 42 below, the relative standard deviation of indenter area in the hardness measurement decreases with penetration depth.

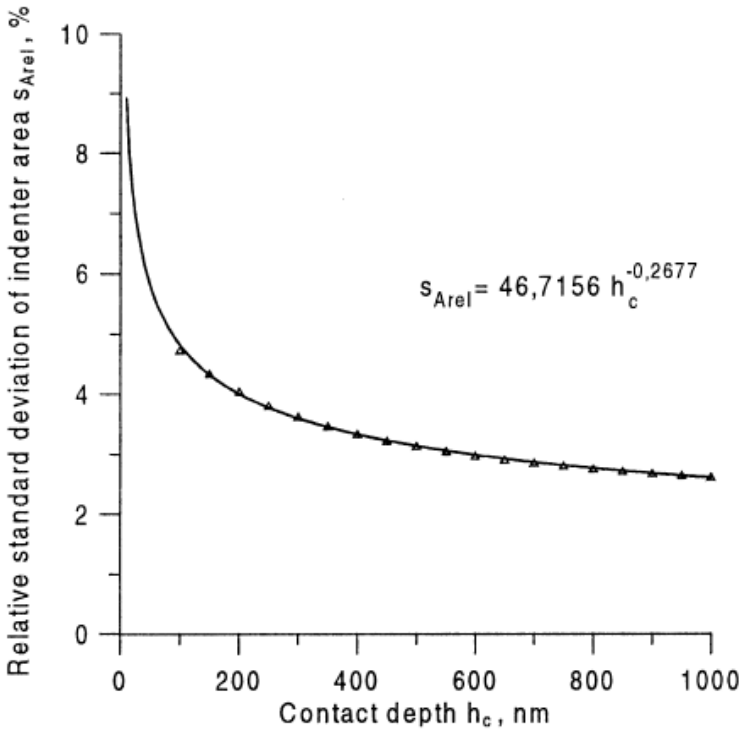

Figure 42. Relative standard deviation of indenter area versus penetration depth [32].

Based on this information, it seems logical to conclude that the percentage error in nanoindentation hardness decreases directly with increases in load. Therefore, in order to decrease the error arising from a constant loading inaccuracy, the value of the peak load should be as high as reasonably possible.

CONSTRAINT FACTOR

An important parameter influencing the hardness is the pressure distribution underneath the indenter. The hardness number (H_{IT}) is determined to be highly dependant on the mean contact pressure, p_m, which is the point when increasing load does not change this pressure. If the material under stress is constrained by the

surrounding matrix, the mean contact pressure must be less than the stress required to initiate yield in compression. As a result, a constraint factor (C) is considered in the hardness determination. The shear stress in the test sample is responsible for local yielding. The material of the sample and the indenter are also influential in determining the constraint factor. For metals having a large E/Y, indentation experiments and theory predict that the constraint factor C is approximately 3 [10]. This assumes the hardness is considered to be equal to the product of the constraint factor and the compressive yield strength,

$$H=CY \tag{7.1}$$

As shown from this definition and proven in research, high hardness values are achieved by large constraint coefficients. Tool steels have high constraint coefficients that are supported by the presence of carbides in the matrix [33].

Inaccuracies in determining both the constraint factor and the hardness can result when there is inadequate spacing between the indentions, or if the specimen is too thin. An inaccuracy can also happen if the indention is made too close to the edge of the sample. In general, the specimen thickness of bulk samples for indentation testing should be at least ten times the indention depth. Another specification states that there should be at least three indention diameters between the centers of the indents or from the sample's edge [3].

In an indentation test there is a stress-strain curve generated by the sample's response. The response is due to undergoing an elastic-plastic deformation cycle. One

source divides this experience into three general regions. Each region is determined by the compressive yield strength (Y) of the material [20].

The first region is characterized by a fully elastic response. This is defined by the mean contact pressure being less than the compressive yield strength, shown in Table 11. Ideally, there will not be a permanent impression in the sample after removing the load. The second region is characterized by the existence of plastic deformation beneath the surface. However, the plastic deformation is constrained by the elastic state of the surrounding material. Therefore, this region is defined where the mean contact pressure is greater than the compressive yield strength, but less than the product of the compressive yield strength and the constraint factor of the material. It is difficult to characterize the states within the second region due to the uncertainty regarding the size and shape of the evolving plastic zone (discussed in the next section). The final region is characterized by a fully plastic response. This is defined by the mean contact pressure being equal to the product involving the compressive yield strength and the constraint factor of the material. The plastic region should continue to grow until the mean contact pressure reaches a maximum value with increasing indenter load. In this region the deformation state depends on the indenter and sample material. Table 11 below shows the information previously discussed in more of a summary format [20].

Table 11. The elastic-plastic deformation cycle simplified into three regions.

$p_m < 1.1 * Y$	Fully elastic region
$1.1 * Y < p_m < C * Y$	Elastic-plastic region
$p_m = C * Y$	Elastic-fully plastic region

CONTACT THEORY

Currently, the most widely accepted theory for quantifying the contact events is the “expanding cavity” theory [34,35]. A modification to this theory involves the penetrated cavity being considered as an incompressible hemispherical core of material, instead of an expansion region under pressure. Therefore, the core pressure is directly proportional to the mean contact pressure. In this model (Figure 43) the indenter surface area in contact with the sample is contained in a hydrostatic core of radius a_c. This core is again contained in a hemispherical plastic zone having radius *c*. A displacement (dh) into the sample will cause an expansion (da). This indenter movement displaces a volume, which is accounted for in the migration of material at the core boundary du(r). This behavior increases the plastic zone (dc) by a certain amount. The radius of the plastic zone increases at the same rate as that of the core [35].

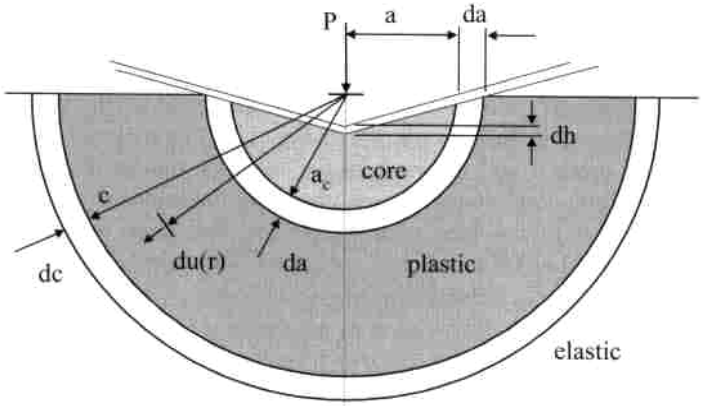

Figure 43. The modified expanding cavity model [10].

Now seems the appropriate time to explain the strategy behind the macroindentation test scale chosen in this research. The Rockwell test has several scales

to choose from, the challenge is to choose the scale that would make the hardness measurements most comparable. This is accomplished by calculating the contact pressure/contact stress between the indenter and the sample during nanoindentation testing. Second is to assume the same contact pressure for the macroindentation test. The required load to use in the macroindentation test in order for the tests to be related by constant contact pressure can then be calculated. The method used to calculate the contact stress at the nano-scale is based on the Hertzian contact stress. This method determines the localized stress that develops when the surfaces are in contact and loaded. Some amount of deformation takes place and is dependent on the elastic modulus of the material. The contact stress is dependant on the normal contact force, the radius of curvature, and elastic moduli of both materials.

Using the nanoindentation test data, the Hertzian contact stress is calculated below. The equations are based on the contact of a sphere and a plane surface.

$$\frac{1}{E^*} = \frac{\left(1 - v^2\right)}{E} + \frac{\left(1 - v'^2\right)}{E'} \tag{7.2}$$

where E^* considers the modulus of the indenter and the specimen, and v' and E' is the Poisson's ratio and elastic modulus of the indenter, respectively.

$$\frac{1}{E^*} = \frac{\left(1 - v^2\right)}{E} + \frac{\left(1 - v'^2\right)}{E'} = \frac{\left(1 - 0.285^2\right)}{200} + \frac{\left(1 - 0.135^2\right)}{851} \quad \therefore \quad E^* = 174\ GPa$$

$$a = \left[\frac{3NR}{4E^*}\right]^{1/3} \tag{7.3}$$

where a is the contact radius between the Berkovich indenter and the sample in mm., N is the max load in newtons, and R is the tip radius in mm.

$$a = \left[\frac{3 * .009 * 2.25\, x10^{-4}}{4 * 174 * 1000} \right]^{1/3} = 2.059\, x10^{-4}\, mm$$

$$\sigma = Hertzian\ Contact\ Stress = \frac{N}{\pi a^2} = 67.574\ GPa \tag{7.4}$$

The contact stress/pressure for the nano-scale test will now be used to determine the proper load in the Rockwell hardness tests. This is found by the following:

$$Contact\ \text{Pr}essure = \frac{N}{a} \quad \therefore \quad N = C.P. * a \tag{7.5}$$

where P is the proper Rockwell load in kg, and a (mm^2) is the apparent area of contact between the sample and the indenter. This variable is found by calculating the apparent contact area of the Berkovich indenter (using test data) and then using a ratio function to yield the apparent Brale indenter contact area.

$$a_{Berk.} = \frac{N}{C.P.} = \frac{0.009N}{3.54GPa} = 2.54\, x10^6\ nm^2$$

$$Ratio: \quad \frac{225\, nm}{2.54\, x10^6\ nm^2} = \frac{200{,}000\, nm}{a_{HR}} \quad \therefore \quad a_{Brale} = 0.00226\, mm^2$$

Finally, the Rockwell test load is determined by using the Hertzian contact stress and the apparent contact area recently determined for the Brale indenter.

$$N = (67.574\, GPa) * (0.00226 mm^2) = 152.7\, N = 15.6\, kg$$

Therefore, the correct Rockwell scale using the Brale indenter that corresponds to the load determined above is the superficial Rockwell N scale. This scale has three load

options (15, 30, and 45 kg). The load used in this research will be the 15 kg load. The correct notation for this hardness test scale is HR15N (e.g. 75.9 HR15N).

RESIDUAL STRESSES

In many materials (including those used in this research) tensile or compressive stresses may be present in the sample as a result of processing (heat treatments) or surface preparation techniques like cold work induced polishing. The shape of the indentation or pile up gives some information about the extent of residual stress within the sample. Many studies have examined the required load to initiate cracks in brittle materials in order to determine the magnitude and direction of surface residual stresses. This is also done to determine the extent of residual stresses from tempering. Additionally, deviations in the shape of the load-displacement response from that expected could also be an indication of residual stresses. However, experiments have shown that the effect is too small to be measured accurately for a compressive stress and a tensile stress compared to the stress-free state [10].

BERKOVICH INDENTER

The indenter used for nanoindentation testing in this research is the Berkovich indenter. A major reason for the development of the Berkovich indenter was to enable accurate testing of very hard materials because of the longer diagonal and steeper surfaces. When very hard materials were tested, the diagonal resulting from the Vickers indention was difficult to measure because of the shallow indention, giving inaccurate

hardness measurements. Another benefit for the Berkovich indenter is that the three-sided pyramid is easier to fabricate than the four-sided Vickers pyramid. This is due to the relative ease of making three edges to meet at a point rather than four. The face angles of the Berkovich indenter were originally 65.03º giving an identical actual surface area to depth ratio as the Vickers indenter. Currently, the face angles are 65.27º corresponding to the same cross-sectional area to depth ratio as the Vickers indenter [36]. The aspect ratio of the Berkovich indenter is 1-to-8. The radius of the tip of the Berkovich indenter in new condition is 50-100 nm, and will mature to about over 200 nm with gentle use. The strain created within the sample using either indenter is approximately 8%. Permitting that the sample surface roughness is less than 50 nm RMS, the Berkovich indenter is the best indenter for most bulk samples [36].

The mean contact pressure for the Berkovich indenter is determined from the quotient of the indenter load (P) and the cross-sectional area of contact, similar to the hardness value. The measured depth of penetration determines the projected cross-sectional area of contact (h_p). Therefore,

$$A_P = 3\sqrt{3}\, h_p^2 \tan^2 \theta \tag{7.6}$$

where $\theta = 65.27$.

This is further simplified to:

$$A_P = 24.5\, h_p^2 \tag{7.7}$$

Therefore, the indentation hardness equation is given below.

$$H_{IT} = P \Big/ 24.5\, h_p^2 \tag{7.8}$$

An elastic-plastic response can be assumed for the Berkovich indenter. Although Figure 9 on page 36 shows that the total displacement can be determined from adding h_p and h_a, it is usually found from analysis of the test data. Dimension h_a is easily found from the unloading curve at maximum load (P).

CORRELATION

In order to reveal the knowledge developed through this research, the hardness values must first be compared. Table 12 consolidates the data for comparison.

Table 12. O1 tool steel hardness test data.

Multi-Scale Indentation Test Data				
	HT 2	HT 1	N-HT 1	Ta
Macroindentation (Hv)	635	459	191	133
Nanoindentation (kg/mm^2)	858 ± 84	732 ± 41	314 ± 15	240

One way to compare the results is to ratio the macroindentation hardness values to the nanoindentation hardness values. This will yield an *indentation correlation factor* (ICF) that can be used to multiply the true nanoindentation hardness values of samples from other nanoindentation tests in order to obtain the Vickers scale hardness values.

$$ICF_{HT2} = \frac{635}{858} = 0.740$$

$$ICF_{HT1} = \frac{459}{732} = 0.627$$

$$ICF_{NHT1} = \frac{191}{314} = 0.608$$

$$ICF_{Ta} = \frac{133}{240} = 0.555$$

First, a benefit of the results in this research is that the test data considers materials over a very broad hardness range. From the computations above it appears that a conclusion could be made concerning a correlation factor for the nanoindentation data. Notice that the factor between heat treated sample 1 and non-heat treated sample 1 is very small. Since less than 5% difference in the nanoindentation data will cause the factors to overlap, the factors are practically equal. Therefore, it can be concluded that for a nanoindentation hardness from ~300 kg/mm^2 up to ~750 kg/mm^2, a factor of 0.620 can be used to yield the standard Vickers hardness value. At ~850 kg/mm^2, a factor of 0.740 can be used to yield the standard Vickers hardness value of ~635 *Hv*. Therefore, equation (7.9) has been developed to determine the hardness of a microstructural feature in the Vickers scale.

$$H_{Hv} = H_{IT} * ICF \tag{7.9}$$

Figure 44 allows identification of all Vickers hardness values graphically. The Vickers (macro-scale) hardness values are determined by first projecting a horizontal line from the nanoindentation hardness value of a sample to the correlation curve. Projecting the intersection down to the x-axis, this will yield the corresponding Vickers macroindentation hardness value. The error in the nanoindentation data begins at 314 kg/mm^2 with 8%, progresses to 9% at 732 kg/mm^2, and spans 10% at 858 kg/mm^2. The error associated with the tantalum sample is less than 1%. As expected, in the graph there are three segmented linear curves with different slopes that make up the correlation

curve. The reason for this is due to the various heat treatments (redistribution of carbides in the matrix) and the ensuing oxidation.

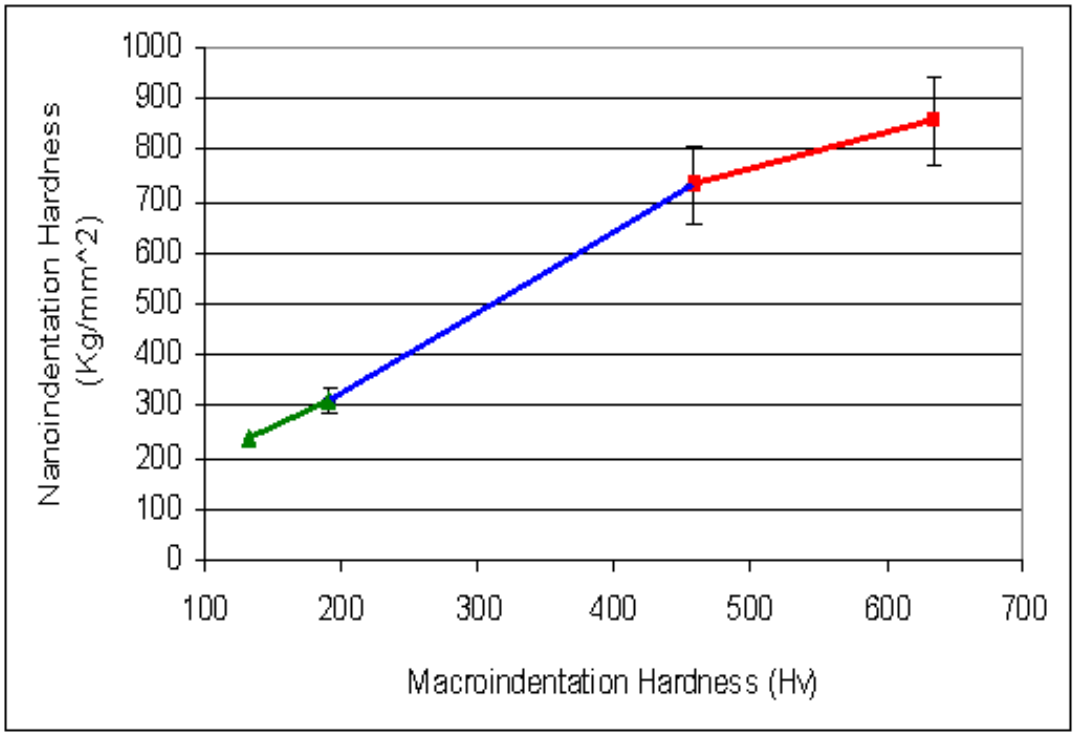

Figure 44. Multi-scale indentation hardness correlation.

CHAPTER VIII

CONCLUSIONS

The objectives of this research were found by selecting and preparing a tantalum sample and O1 tool steel samples with various heat treatments. The resulting test data was used to develop multiplicative factors for the materials chosen. Additionally, a correlation graph was developed from the test data. As a result, Vickers hardness values can be assigned to features that are too small to be precisely tested by the conventional macro/microindentation hardness testing techniques.

Obtaining Vickers hardness values from nanoindentation hardness values can now be done using two methods. One method may be used by using equation (7.9) derived in this thesis and applying the multiplicative factors found in the Correlation section on page 88 in this thesis. For example, nanoindentation hardness results of a 300 series stainless steel sample may be correlated to the Vickers scale by multiplying the hardness data by 0.620 (for samples believed to range from 200 Hv – 460 Hv).

Another method may be used to determine the Vickers hardness by projecting a horizontal line corresponding to the nanoindentation hardness of a sample to the correlation curve in Figure 44 on page 90 of this thesis. That intersection can then be projected down to the x-axis yielding the corresponding Vickers value. The correlation between nano and macroindentation hardness values is a linear relationship. A factor known as the indentation correlation factor (ICF) was derived in this thesis. This thesis may also serve as a research methodology for correlating hardness data for materials other than metals.

As mentioned earlier, this research is anticipated to impact the pipeline division of the petroleum industry and ultimately may help to mitigate the United States current supply issues of oil and natural gas, thereby helping to reduce the price of gasoline. This will be accomplished by implementing the standard nanoindentation test method and applying the correlation recommended here in order to improve the petroleum industry's understanding of microstructural features in the FSW weld nugget. The new information gained may lead to the FSW technique replacing the liquid-state fusion welding of pipelines in extreme environments, which will improve the project economics for developing oil and gas fields. The improved economics are a result of the FSW technique having no consumables, requiring less set-up costs, and creating a lower environmental impact. These factors are in addition to optimizing pipeline up-time as a result of the stronger welds. The improved economics would then support more oil and gas field developments, thereby increasing oil and gas supply rates. This boost in available energy would then offset the cost to consumers as a result of enhancing the energy supply.

Future research may involve preparing more 01 tool steel samples with specific hardness values within the range studied in this thesis. This work would strengthen the correlation by populating the existing curve with more data points. Further research may also be pursued in order to extend the correlation curve to include samples with hardness values greater than those tested in this thesis. This research may also be advanced by using the methodology presented in this thesis to develop hardness correlations for materials other than metals.

REFERENCES

[1] Jones, D. A., 1996, *Principles and Prevention of Corrosion,* 2nd ed., Pearson Education, Inc., Upper Saddle River, NJ, p. 3.

[2] Mott, B. W., 1956, *Micro-Indentation Hardness Testing*, Butterworths Scientific Publications, London.

[3] Callister, W. D., 2003, *Materials Science and Engineering An Introduction,* Sixth ed., John Wiley & Sons, Inc, Hoboken, NJ.

[4] Material Property Data, (3/20/2008), "Metals search for tantalum characteristics," http://www.matweb.com.

[5] Budinski, K. G., Budinski, Michael K., 2005, *Engineering Materials: Properties & Selection*, 8th ed., Pearson Education, Inc., Upper Saddle River, NJ, p. 483.

[6] Tool Steel and Specialty Alloy Selector, (1/20/2008), "Tool steel information," http://www.crucibleservice.com.

[7] ASTM A 681-07, "Standard Specification for Tool Steels Alloy," ASTM International, West Conshohocken, PA.

[8] ASTM E 18-08, "Standard Test Methods for Rockwell Hardness of Metallic Materials," ASTM International, West Conshohocken, PA.

[9] Wilson Instruments, (3/18/2008), "Series 2000 brochure," www.wilsoninstruments.com.

[10] Fischer-Cripps, A. C., 2004, *Nanoindentation*, 2nd ed., Springer, New York.

[11] ISO 14577: 2002, "Metallic Materials-instrumented Indentation Test for Hardness and Materials Parameters," International Organization for Standardization, Geneva, Switzerland.

[12] Hysitron, 2001, *Triboindenter® User Manual*, Hysitron Inc., Minneapolis, MN.

[13] Li, M., Zhang, T.-h., Gan, C.-h., Liang, N.-g., 2002, "Hardness testing on surface layer of material and results analyzing contrastively," Chinese J. of Aeronautics **15**(2), pp. 82-89.

[14] Nix, W. D., Gao, H., 1998, "Indentation size effects in crystalline materials: a law for strain gradient plasticity," J. Mech. Phys. Solids, **46**, pp. 411-425.

[15] Zong, Z., Lou, J., Adewoye, O. O., Elmustafa, A. A., Hammad, F., Soboyejo, W. O., 2006, "Indentation size effects in the nano- and micro-hardness of fcc single crystal metals," Mater. Sci. Eng.**, A434**, pp. 178-187.

[16] Chicot, D. Roudet, F. Soom, A. Lesage, J., 2007, "Interpretation of instrumented hardness measurements on stainless steel with different surface preparations," Surf. Eng., **23**(1), pp. 32-39.

[17] Nagy, P., Csanady, A., Vero, B., Palinkas, G., Kalman, E., 2003, "The combined application of nanoindentation and scanning probe microscopy in materials science," Mater. Sci. Forum, **414-415**, pp. 297-303.

[18] Mehl, R., 1972, *Metals Handbook Volume 7: Atlas of Microstructures of Industrial Alloys*, 8th ed., edited by T. Lymon, ASM Int'l, Materials Park, OH.

[19] ASTM E 140-07, "Standard Hardness Conversion Tables for Metals Relationship Among Brinell Hardness, Vickers Hardness, Rockwell Hardness, Superficial Hardness, Knoop Hardness, and Scleroscope Hardness," ASTM International, West Conshohocken, PA.

[20] Tabor, D., 1951, *The Hardness of Metals*, Clarendon Press, Oxford.

[21] Qian, L., Li, M., Zhou, Z., Yang, H., Shi, X., 2005, "Comparison of nano-indentation hardness to microhardness," Surf. Coat. Technol.**, 195**, pp. 264-271.

[22] Elmustafa, A. A., Stone, D. S., 2002, "Indentation size effect in polycrystalline F.C.C. metals," Acta Mater., **50**, pp. 3641-3650.

[23] Samuels, L. E., 1986, "Microindentation in metals," ASTM STP 889, ASTM Int'l, Philadelphia, pp. 5-25.

[24] Sargent, P. M., 1986, "Use of the indentation size effect on microhardness for materials characterization," ASTM STP 889, ASTM Int'l, Philadelphia, pp. 160-174.

[25] Li, H., Ghosh, A., Han, Y. H., Bradt, R. C., 1993, "The frictional component of the indentation size effect in low load microhardness testing," J. Mater. Res., **8**, pp. 1028-1032.

[26] Ma, Q., Clarke, D. R., 1995, "Size dependent hardness in silver single crystals," J. Mater. Res., **10**, pp. 853-863.

[27] DeGuzman, M. S., Neubauer, G., Flinn, P., Nix, W. D., 1993, "The role of indentation depth on the measured hardness of materials," Mater. Res. Symp. Proc. 308, Materials Research Society, Pittsburgh, PA, pp. 613-618.

[28] Fleck, N. A., Muller, G. M., Ashby, M. F., Hutchinson, J. W., 1994, "Strain gradient plasticity: theory and experiment," Acta Metall. Mater., **42**, pp. 475-487.

[29] McElhaney, K. W., Vlassak, J. J., Nix, W. D., 1998, "Determination of indenter tip geometry and indentation contact area for depth-sensing indentation experiments," J. Mater. Res., **13**, pp. 1300-1306.

[30] Poole, W. J., Ashby, M. F., Fleck, N. A., 1996, "Microhardness of annealed and work-hardened copper polycrystals," Scripta Metall. Mater., **34**, pp. 559-564.

[31] Zhang, T.-Y., Zu, W.-H., 2002, "Surface effects on nanoindentation," J. Mater Res.**, 17**(7), pp. 1715-1720.

[32] Herrmann, K., Hasche, K., Pohlenz, F., Seemann, R., 2001, "Characterization of the geometry of indenters used for the micro- and nanoindentation method," Measurement, **29**, pp. 201-207.

[33] Hirukawa, H., Matsuoka, S., Miyahara, K., Furuya, Y., 2003, "Nanoscopic strength analysis of tempered-martensitic steels using atomic force microscopy and nanoindentation," Mater. Lett., **58**, pp. 321-325.

[34] Johnson, K. L., 1970, "The correlation of indentation experiments," J. Mech. Phys. Sol., **18**, pp. 115-126.

[35] Johnson, K. L., 1985, *Contact Mechanics*, Cambridge University Press, Cambridge, MA.

SUPPLEMENTAL SOURCES CONSULTED

ASTM International, (2/11/2008), "Standards search," http://www.astm.org.

Elmustafa, A. A., Stone, D. S., 2003, "Nanoindentation and the indentation size effect: Kinetics of deformation and strain gradient plasticity," J. Mech. Phys. Sol., **51**, pp. 357-381.

Elmustafa, A. A., Stone, D. S., 2003, "Stacking fault energy and dynamic recovery: do they impact the indentation size effect?," Mater. Sci. Eng., **A358**, pp. 1-8.

International Organization for Standardization, (2/15/2008), "Standards search," http://www.iso.org.

Lawn, B. R., Hockey, B. J., Weiderhorn, S. M., 1980, "Thermal effects in sharp-particle impact," J. Amer. Ceram. Soc., **63**(5-6), pp. 356-358.

Pharr, G. M., Bolshakov, A., 2002, "Understanding indentation unloading curves," J. Mater. Res., **17**(10), pp. 2660-2671.

Qu, S., Huang, Y., Nix, W. D., Jiang, H., Zhang, F., Hwang, K. C., 2004, "Indenter tip radius effect on the Nix-Gao relation in micro- and nanoindentation hardness experiments," J. Mater. Res.**, 19**(11), pp. 3423-3434.

VITA

Damon Wade Bennett received his Bachelor of Science degree in mechanical engineering technology from Oklahoma State University at Stillwater in 2004. He entered the Mechanical Engineering program at Texas A&M University in August 2006. His research interests include nano-scale characterization of the chemical, mechanical, physical, and tribological properties of surfaces and interfaces of materials. After graduation he plans to continue to work in the petroleum industry.

Mr. Bennett may be reached at ExxonMobil Production Company, 396 West Greens Road, Houston, TX 77067. His email is d9benn2@tamu.edu.